


Incorporating peridynamic differential operator into Carrera unified formulation for beam type structures

Jing Zhang^a , Erdogan Madenci^b, and Yijun Liu^a

^aDepartment of Mechanics and Aerospace Engineering, Southern University of Science and Technology, Shenzhen, China; ^bDepartment of Aerospace and Mechanical Engineering, University of Arizona, Tucson, Arizona, USA

ABSTRACT

This study introduces an approach for the solution of governing equations resulting from Carrera unified formulation (CUF) by incorporating the peridynamic differential operator (PDDO). The theoretical foundation integrates the 1D PDDO formulation with the unified theory of refined beam models. The 3D mathematical/physical surfaces are reconstructed *via* Taylor/Lagrange expansions of cross-sectional coordinates. The bond-wise PDDO fundamental nuclei are developed for nonlocal integration, which remains invariant with respect to the expansion order across the beam cross-section. The capability of the proposed approach for 3D analysis is demonstrated through static simulations of beams with various geometries under prescribed displacement and traction boundary conditions. The predicted 3D deformation states are in agreement with analytical solutions and finite element method results, confirming the accuracy and robustness of the formulation.

ARTICLE HISTORY

Received 2 March 2026
Accepted 27 March 2026

KEYWORDS

Carrera unified formulation; peridynamic differential operator; nonlocal mechanics; dimensionally reduced approach; beam-type structures

1. Introduction

The finite element method (FEM) is widely recognized for its effectiveness and versatility in analyzing structural components. Its prevalence stems from two major developments: the formulation of mathematical methods for solving differential equations in approximate or weak forms and the advent of computational tools capable of automating these operations on digital computers [1]. In FEM, the computational domain is discretized into finite elements, within which the governing equations are solved, and global deformation and stress fields are obtained through systematic assembly procedures. However, FEM solutions based on classical continuum mechanics (CCM) encounter significant challenges in the presence of discontinuities within the material body. When geometric or material discontinuities exist, extremely refined meshes are often required to achieve convergence and accuracy. Moreover, as cracks propagate, additional treatments—such as cohesive elements, enrichment functions, or adaptive remeshing—are necessary to accommodate evolving discontinuities. Similarly, meshfree methods derived from CCM, including smoothed particle hydrodynamics and the reproducing kernel particle method, also require supplementary measures such as smoothness assumptions or kernel-function reconstruction to manage spatial derivatives and associated approximations effectively [2].

To provide a unified framework for modeling both continuous media and cracks, peridynamics (PD) eliminates the

principle of local action inherent in CCM and establishes a nonlocal continuum theory that explicitly accounts for long-range interactions [3–5]. The governing equation of PD takes an integro-differential form, which imposes no smoothness requirements on the field variables. Consequently, PD remains physically and mathematically consistent in both continuous and discontinuous domains, making it particularly suitable for damage and fracture analysis across multiple length scales [6–8]. Building upon the concept of PD interactions, the PD differential operator (PDDO), introduced in 2016 [2,9], enables numerical differentiation through integration. By reestablishing nonlocal interactions between a point and its surrounding neighborhood, the PDDO allows for accurate evaluation of field variables and their derivatives at discrete points without explicit differentiation—maintaining validity even in the presence of jump discontinuities or singularities. Acting as a bridge between local and nonlocal theories, PDDO facilitates numerical analysis over smooth or scattered data while addressing several limitations previously identified in PD formulations [10–15]. Applications of PDDO extend from static and dynamic analyses of brittle and ductile materials to multiscale and multifield problems [10,16–19]. Nonetheless, when applied to structures with pronounced one-dimensional (1D) characteristics, models that consist of PD particles can present computational challenges. Simplified 1D models often lose critical cross-sectional information [20,21], whereas fully three-dimensional (3D) nonlocal models may lead to excessive discretization in the longitudinal direction.

To address the limitations of simplified 1D PD models, the PDDO has been increasingly integrated with structural theories to capture 3D behaviors of beam structures, owing to its simplicity, compatibility with PD, and ability to model failure. Aung et al. [22] introduced two PD formulations based on the Euler–Bernoulli beam theory for planar, arbitrarily curved beams, while Nguyen et al. [23] combined the kinematic assumptions of the Timoshenko–Ehrenfest beam theory with PDDO to simulate the static, dynamic, and fracture responses of curved beams. Li et al. [24] performed large-deformation analyses of functionally graded beams with linearly varying and parabolic lower surfaces using PDDO. Madenci et al. [25] applied the PDDO to solve the equilibrium equations of the refined zigzag theory (RZT) for predicting the progressive failure of laminated composite structures. Dorduncu [26] further coupled RZT with PDDO for the stress analysis of laminated composite beams, and later developed a nonlocal beam model by combining the PD least-squares minimization method with RZT to investigate the stress and deformation states of adhesively bonded beams with functionally graded adhesive layers [27]. More recently, Zhang et al. [28] coupled Carrera unified formulation (CUF) and PDDO for beam and plate structures that reproduces exact 3D deformation states using 1D and 2D PDDO models that do not involve nonlocal surface or boundary corrections. Distinct from earlier formulations, this approach reconstructs the 3D mathematical surfaces of slender structures through a Taylor series (TS) expansion of cross-sectional coordinates in accordance with CUF. CUF offers a compact and systematic notation through which classical and refined high-order beam, plate, and shell theories can be consistently derived and solved. Its governing equations are expressed in terms of fundamental nuclei (FN), which remain independent of the order and class of approximation functions used in the expanded directions [29,30]. The FN extraction feature allows CUF to be efficiently implemented for automated computation. When incorporated into finite element frameworks, CUF has been successfully applied to the static and dynamic analyses of beams, plates and shells with or without geometric or constitutive nonlinearities [31–34]. Its integration with nonlocal methods [35–39] further demonstrates its capability to extend one- and 2D nonlocal models to their 3D counterparts, confirming its strong compatibility with PD and PDDO theories.

The present study reconstructs both mathematical and physical 3D surfaces of beam-type structures. The mathematical surfaces are generated through the Taylor expansion class, whereas the physical surfaces are obtained *via* the Lagrange expansion class, enabling the framework to accommodate a wider range of practical structural configurations in comparison to the previous work [28]. Incorporating physical surface conformity enhances the consistency of the proposed formulation with classical FEM and PD analyses, both of which rely on abstract entities such as lines or reference surfaces for model construction. Through Taylor and Lagrange expansions of cross-sectional parameters, the present approach enables exact 3D analysis using a 1D PDDO model. The capability and accuracy of the proposed approach are demonstrated through benchmark tests on

beam stretching and bending problems involving various cross-sectional geometries.

2. Peridynamic differential operator

PDDO conducts numerical analysis making use of discrete data and provides a unified solution to differential and integral equations regardless of their intrinsic behavior and presence of singularity. It is constructed by establishing a set of orthogonal PD functions which stays in effect regardless of the symmetry of the PD horizon. The following section elaborates on the derivation of PD functions and the construction of PDDO.

As shown in Figure 1, a material body is discretized into multiple material particles in domain \mathcal{D} . The particle \mathbf{x} generates interactions with its neighbor particles \mathbf{x}' within a certain cutoff distance called the horizon $\mathcal{H}_{\mathbf{x}}$. The horizon can be asymmetric or symmetric for the construction of PDDO. The relative position vector bonding \mathbf{x} and \mathbf{x}' is defined as $\boldsymbol{\xi} = \mathbf{x}' - \mathbf{x}$. According to Madenci et al. [9,25], the PDDO is constructed using N -th order TS of a scalar field $f(\mathbf{x}') = f(\mathbf{x} + \boldsymbol{\xi})$ as

$$\frac{\partial^p f(\mathbf{x})}{\partial x^p} = \int_{\mathcal{H}_{\mathbf{x}}} f(\mathbf{x} + \boldsymbol{\xi}) g_N^p(\boldsymbol{\xi}) dV, \quad (1)$$

where p denotes the order of differentiation with respect to x . The orthogonality property of PD functions requires

$$\frac{1}{n!} \int_{\mathcal{H}_{\mathbf{x}}} \xi^n g_N^p(\boldsymbol{\xi}) dV = \delta_{np}, \quad (2)$$

where $n, p = 0, 1, \dots, N$. Such orthogonality property permits the determination of any order of derivatives of the spatial functions. PD function $g_N^p(\boldsymbol{\xi})$ can then be written as

$$g_N^p(\boldsymbol{\xi}) = \sum_{q=0}^N a_q^p w_q(|\boldsymbol{\xi}|) \xi^q, \quad (3)$$

where $w_q(|\boldsymbol{\xi}|)$ are the weight functions associated with each term ξ^q . The unknown coefficients, a_q^p can be obtained from the solution of

$$\sum_{q=0}^N A_{nq} a_q^p = b_n^p. \quad (4)$$

The coefficient matrix A is constructed as

$$A_{nq} = \int_{\mathcal{H}_{\mathbf{x}}} w_q(|\boldsymbol{\xi}|) \xi^{n+q} dV \quad (5)$$

and vector b is defined as

$$b_n^p = n! \delta_{np}, \quad (6)$$

where δ_{np} is the Kronecker symbol.

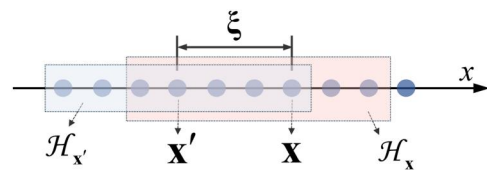


Figure 1. PD interaction for 1D analysis.

For 1D analysis, the PDDO expression for derivatives up to 2nd order can be written as

$$\begin{pmatrix} f(\mathbf{x}) \\ \frac{\partial f(\mathbf{x})}{\partial x} \\ \frac{\partial^2 f(\mathbf{x})}{\partial x^2} \end{pmatrix} = \int_{H_x} f(\mathbf{x} + \xi) \begin{pmatrix} g_2^0(\xi) \\ g_2^1(\xi) \\ g_2^2(\xi) \end{pmatrix} dV, \quad (7)$$

which can be recast in the form of

$$\begin{pmatrix} \frac{\partial f(\mathbf{x})}{\partial x} \\ \frac{\partial^2 f(\mathbf{x})}{\partial x^2} \end{pmatrix} = \int_{H_x} (f(\mathbf{x} + \xi) - f(\mathbf{x})) \begin{pmatrix} g_2^1(\xi) \\ g_2^2(\xi) \end{pmatrix} dV. \quad (8)$$

Similar to PD interactions, PDDO ensures the determination of field variables and their derivatives using PD models, without symmetry requirements on PD horizon. As the size of horizon decreases or the number of terms in PD function increases, PDDO recovers the local differentiation.

3. CUF for beam type structures

The unified formulation solves the elasticity problem by generating hierarchical approximated solution on the basis of fundamental nuclei with the expansion order as the only input parameter. Its combination with PDDO contributes to an effective dimensionally reduced approach for the restoration of 3D deformation states of beam structures. The establishment of the unified formulation based on high-order beam theory and PDDO is elaborated in the following section.

3.1. The unified formulation for beam structures

The unified formulation of the cross-section displacement field is described by an expansion of generic functions F_s ,

$$\mathbf{u} = F_s \mathbf{u}_s, s = 1, 2, \dots, M, \quad (9)$$

where $\mathbf{u} = \{u_x \ u_y \ u_z\}^T$ is the 3D displacement vector, while $\mathbf{u}_s = \{u_{x_s} \ u_{y_s} \ u_{z_s}\}^T$ is the τ th order generalized displacement vector. M stands for the number of expanded terms. For beam type structures (Fig. 2), Equation (9) is written as

$$\mathbf{u}(x, y, z) = F_s(x, z) \mathbf{u}_s(y), s = 1, 2, \dots, M, \quad (10)$$

where F_s are functions of the cross-section coordinates x and z . The choice of the expansion function F_s or the number of terms depends on the practical conditions and the required degree of accuracy. Possible choices include Taylor polynomials, Lagrange polynomials, etc [31].

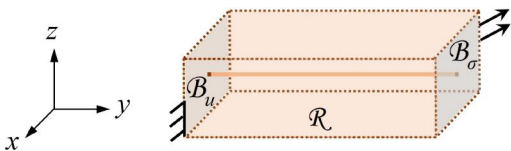


Figure 2. 3D model expanded from 1D PDDO model.

The Taylor expansion class (Figure 3) presents a unified approach to deal with beam theories of any order. The 3D displacement fields are obtained through a single formal expression constructed on the basis of Taylor-like polynomials (Table 1) in a unified manner, with the expansion order N as the only input parameter. The notation PDDO(TE_ N) is utilized to denote beam-type structures expanded by N -th order Taylor polynomials.

For instance, the displacement field of PDDO(TE_2) model is established as

$$\begin{aligned} u_x(x, y, z) &= u_{x_1}(y) + xu_{x_2}(y) + zu_{x_3}(y) + x^2u_{x_4}(y) + xzu_{x_5}(y) + z^2u_{x_6}(y) \\ u_y(x, y, z) &= u_{y_1}(y) + xu_{y_2}(y) + zu_{y_3}(y) + x^2u_{y_4}(y) + xzu_{y_5}(y) + z^2u_{y_6}(y) \\ u_z(x, y, z) &= u_{z_1}(y) + xu_{z_2}(y) + zu_{z_3}(y) + x^2u_{z_4}(y) + xzu_{z_5}(y) + z^2u_{z_6}(y). \end{aligned} \quad (11)$$

As a kind of centered expansion, TE creates a mathematical 3D surface along the axial coordinate y . The number of expansion terms can be adjusted to fulfill the given accuracy requirement, while the richer expansion contributes to a more accurate result. The 3D deformation details at a specific point can be obtained through proper postprocessing based on the formulation Equation (9).

The Lagrange expansion class (Figure 4) takes pure displacement components as unknown variables and uses Lagrange polynomials to expand the displacement fields across the section. The notation PDDO(LE_ $\zeta \times \eta$ L β) is utilized for beams with square cross-sections where ζ and η denote the number of β -point Lagrange elements in x direction and z direction. The notation PDDO(LE_ θ L β) is utilized for those with thin-walled cross-sections where θ denote the total number of β -point Lagrange elements. For nine-point Lagrange (L9) element, the expansion function F_s and the point coordinates are given in Equation (12) and Table 2.

$$\begin{aligned} F_s &= \frac{1}{4}(r^2 + rr_s)(s^2 + ss_s), s = 1, 3, 5, 7 \\ F_s &= \frac{1}{2}s_s^2(s^2 + ss_s)(1 - r^2) + \frac{1}{2}r_s^2(r^2 + rr_s)(1 - s^2), s = 2, 4, 6, 8 \\ F_s &= (1 - s^2)(1 - r^2), s = 9 \end{aligned} \quad (12)$$

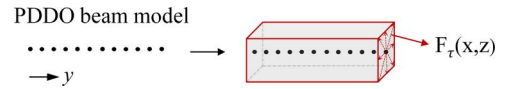


Figure 3. 3D PDDO(TE) model.

Table 1. Taylor-like polynomials.

N	M	F_s
0	1	$F_1 = 1$
1	3	$F_2 = x, F_3 = z$
2	6	$F_4 = x^2, F_5 = xz, F_6 = z^2$
3	10	$F_7 = x^3, F_8 = x^2z, F_9 = xz^2, F_{10} = z^3$
...
N	$(N+1)(N+2)/2$	$F_{(N^2+N+2)/2} = x^N, \dots, F_{(N+1)(N+2)/2} = z^N$

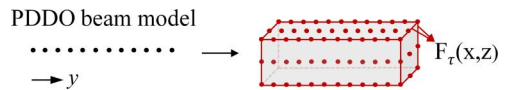


Figure 4. 3D PDDO(LE) model.

Table 2. Normalized coordinates of L9 points.

Point	r_s	s_s
1	-1	-1
2	0	-1
3	1	-1
4	1	0
5	1	1
6	0	1
7	-1	1
8	-1	0
9	0	0

where r and s are the normalized coordinates. r_s and s_s are the coordinates of nine nodes in L9 elements. Different from TE class, LE creates a physical 3D surface, where the 3D deformation details are directly solved from the governing equations. With its model variables and boundary conditions being directly applied on the physical surface, LE models are particularly suitable for locally refined or CAD-coupled scenarios. Moreover, a finer cross-section mesh (high order models) can be used for more accurate results.

By means of the principle of virtual displacement (PVD), the governing equations of high order beam theories can be derived and written in general as

$$\begin{cases} \mathbf{K}^{\tau s} \mathbf{u}_s = \mathbf{P}^\tau, \mathbf{x} \in \mathcal{R} \\ \mathbf{\Pi}^{\tau s} \mathbf{u}_s = \bar{\mathbf{p}}^\tau, \mathbf{x} \in \mathcal{B}_\sigma \\ \mathbf{u}_s = \bar{\mathbf{u}}_s, \mathbf{x} \in \mathcal{B}_u \end{cases} \quad (13)$$

where $\tau, s = 1, 2, \dots, N$. $\mathbf{K}^{\tau s}$ and $\mathbf{\Pi}^{\tau s}$ are FNs for inner domain \mathcal{R} and boundary domain \mathcal{B}_σ and \mathcal{B}_u (Figure 2), whose derivation is elaborated in Appendix A. \mathbf{P} denotes generalized forces, while $\bar{\mathbf{p}}$ and $\bar{\mathbf{u}}$ stand for the applied traction and displacement boundaries. The governing equations in expansion form are

$$\begin{aligned} \delta u_{x\tau} &: \left(J_{\tau,x^s,x}^{11} + J_{\tau,z^s,z}^{55} \right) u_{xs} - J_{\tau s}^{66} u_{xs,yy} + \left(J_{\tau,x^s}^{12} - J_{\tau s,x}^{66} \right) u_{ys,y} + \left(J_{\tau,x^s,z}^{13} + J_{\tau,z^s,x}^{55} \right) u_{zs} = P_x^\tau \\ \delta u_{y\tau} &: \left(J_{\tau,x^s}^{66} - J_{\tau s,x}^{12} \right) u_{xs,y} + \left(J_{\tau,x^s,x}^{66} + J_{\tau,z^s,z}^{44} \right) u_{ys} - J_{\tau s}^{22} u_{ys,yy} + \left(J_{\tau,z^s}^{44} - J_{\tau s,z}^{23} \right) u_{zs,y} = P_y^\tau \\ \delta u_{z\tau} &: \left(J_{\tau,x^s,z}^{55} + J_{\tau,z^s,x}^{13} \right) u_{xs} + \left(J_{\tau,x^s}^{23} - J_{\tau s,x}^{44} \right) u_{ys,y} + \left(J_{\tau,x^s,x}^{55} + J_{\tau,z^s,z}^{33} \right) u_{zs} - J_{\tau s}^{44} u_{zs,yy} = P_z^\tau \end{aligned} \quad (14)$$

On the boundary there are

$$\begin{aligned} J_{\tau s}^{66} n_y u_{xs,y} + J_{\tau s,x}^{66} n_y u_{ys} &= \bar{p}_x^\tau \\ J_{\tau s,x}^{12} n_y u_{xs} + J_{\tau s}^{22} n_y u_{ys,y} + J_{\tau s,z}^{23} n_y u_{zs} &= \bar{p}_y^\tau \\ J_{\tau s,z}^{44} n_y u_{ys} + J_{\tau s}^{44} n_y u_{zs,y} &= \bar{p}_z^\tau \end{aligned} \quad (15)$$

The generic terms $J_{\tau,\theta^s,\zeta}^{\alpha\beta}$ are the cross-sectional moment parameters defined as an integral over cross-section Ω , $J_{\tau,\theta^s,\zeta}^{\alpha\beta} = \int_{\Omega} C_{\alpha\beta} F_{\tau,\theta} F_{s,\zeta} d\Omega$. $C_{\alpha\beta}$ are material constants and the suffix after the comma denotes partial derivatives.

3.2. The unified formulation for beam structures with PDDO

To establish the PDDO beam model, the domain \mathcal{D} is spatially discretized into T_{PD} material particles in y -direction, which consists of inner domain \mathcal{R} and boundary domain \mathcal{B} . The boundary domain \mathcal{B} can be further divided into \mathcal{B}_u and \mathcal{B}_σ according to the type of boundaries (displacement boundary or traction boundary), as shown in Figure 2. Each particle $\mathbf{x}^{(k)}$ possesses the volume $V^{(k)}$, mass density $\rho^{(k)}$ and $T^{(k)}$ neighbor particles labeled as $\mathbf{x}^{(j)}$ within horizon $\mathcal{H}_{\mathbf{x}^{(k)}}$. Particle k is located by coordinate $(x^{(k)}, y^{(k)}, z^{(k)})$. The relative position vector between $\mathbf{x}^{(k)}$ and $\mathbf{x}^{(j)}$ is $(\xi_{x(j)(k)}, \xi_{y(j)(k)}, \xi_{z(j)(k)})$. The expansion order N is the only input parameter determined according to the actual accuracy requirement.

For particle $\mathbf{x}^{(k)}$, $k = 1, 2, \dots, T_{PD}$, the governing equations are

$$\begin{cases} \mathbf{K}^{\tau s}(\xi_{(j)(k)}) \mathbf{u}_s(\mathbf{x}^{(j)}, \mathbf{x}^{(k)}, t) = \mathbf{P}^\tau, \mathbf{x}^{(k)} \in \mathcal{R} \\ \mathbf{\Pi}^{\tau s}(\xi_{(j)(k)}) \mathbf{u}_s(\mathbf{x}^{(j)}, \mathbf{x}^{(k)}, t) = \bar{\mathbf{p}}^\tau, \mathbf{x}^{(k)} \in \mathcal{B}_\sigma \\ \mathbf{u}_s(\mathbf{x}^{(j)}, \mathbf{x}^{(k)}, t) = \bar{\mathbf{u}}_{(k)s}, \mathbf{x}^{(k)} \in \mathcal{B}_u \end{cases} \quad (16)$$

where $\tau, s = 1, 2, \dots, N$. $\mathbf{K}^{\tau s}$ and $\mathbf{\Pi}^{\tau s}$ are the FNs of stiffness matrix established for the inner domain and boundary layer, respectively. \mathbf{u}_τ is the generalized displacement vector for PD particles. Displacement boundaries $\bar{\mathbf{u}}_\tau$ and traction boundaries $\bar{\mathbf{p}}^\tau$ are directly applied on the boundary layer as

$$\begin{aligned} \mathbf{P}^s &= \left\{ \mathbf{P}_{(1)}^s, \mathbf{P}_{(2)}^s, \dots, \bar{\mathbf{p}}_{(j)}^s, \dots, \mathbf{P}_{(k)}^s, \dots, \mathbf{P}_{(T_{PD})}^s \right\} \\ \mathbf{P}_{(k)}^s &= \left\{ P_{(k)}^1, P_{(k)}^2, \dots, P_{(k)}^n, \dots, P_{(k)}^N \right\} \\ \bar{\mathbf{p}}_{(j)}^s &= \left\{ P_{(j)}^1, P_{(j)}^2, \dots, \bar{p}_{(j)}^n, \dots, P_{(j)}^N \right\} \end{aligned} \quad (17)$$

$$\begin{aligned} \mathbf{u}_\tau &= \left\{ \mathbf{u}_{(1)\tau}, \mathbf{u}_{(2)\tau}, \dots, \bar{\mathbf{u}}_{(j)\tau}, \dots, \mathbf{u}_{(k)\tau}, \dots, \mathbf{u}_{(T_{PD})\tau} \right\} \\ \mathbf{u}_{(k)\tau} &= \left\{ u_{(k)1}, u_{(k)2}, \dots, u_{(k)n}, \dots, u_{(k)N} \right\} \\ \bar{\mathbf{u}}_{(j)\tau} &= \left\{ u_{(j)1}, u_{(j)2}, \dots, \bar{u}_{(j)n}, \dots, u_{(j)N} \right\}. \end{aligned} \quad (18)$$

For beam-type models, the PDDO is the function of $\xi_{y(j)(k)}$. According to the PD functions defined in Equation (7), Equation (14) can be recast in PDDO form as

$$\sum_{j=1}^{N(k)} \left\{ \begin{aligned} &u_{xs}(y^{(j)}) \left(J_{\tau,x^s,x}^{11} + J_{\tau,z^s,z}^{55} \right) g_2^0(\xi_{y(j)(k)}) - \left(u_{xs}(y^{(j)}) - u_{xs}(y^{(k)}) \right) J_{\tau s}^{66} g_2^2(\xi_{y(j)(k)}) \\ &+ \left(u_{ys}(y^{(j)}) - u_{ys}(y^{(k)}) \right) \left(J_{\tau,x^s}^{12} - J_{\tau s,x}^{66} \right) g_2^1(\xi_{y(j)(k)}) \\ &+ u_{zs}(y^{(j)}) \left(J_{\tau,x^s,z}^{13} + J_{\tau,z^s,x}^{55} \right) g_2^0(\xi_{y(j)(k)}) \end{aligned} \right\} \Delta L_{(j)} = P_x^\tau \quad (19)$$

$$\sum_{j=1}^{N(k)} \left\{ \begin{array}{l} (u_{xs}(y(j)) - u_{xs}(y(k))) (J_{\tau, x^s}^{66} - J_{\tau s, x}^{21}) g_2^1(\xi_{y(j)(k)}) \\ + u_{ys}(y(j)) (J_{\tau, z^s, z}^{44} + J_{\tau, x^s, x}^{66}) g_2^0(\xi_{y(j)(k)}) - (u_{ys}(y(j)) - u_{ys}(y(k))) J_{\tau s}^{22} g_2^2(\xi_{y(j)(k)}) \\ + (u_{zs}(y(j)) - u_{zs}(y(k))) (J_{\tau, z^s}^{44} - J_{\tau s, z}^{23}) g_2^1(\xi_{y(j)(k)}) \end{array} \right\} \Delta L_{(j)} = P_y^{\tau} \quad (20)$$

$$\sum_{j=1}^{N(k)} \left\{ \begin{array}{l} u_{xs}(y(j)) (J_{\tau, z^s, x}^{31} + J_{\tau, x^s, z}^{55}) g_2^0(\xi_{y(j)(k)}) \\ + (u_{ys}(y(j)) - u_{ys}(y(k))) (J_{\tau, z^s}^{32} - J_{\tau s, z}^{44}) g_2^1(\xi_{y(j)(k)}) \\ + u_{zs}(y(j)) (J_{\tau, z^s, z}^{33} + J_{\tau, x^s, x}^{55}) g_2^0(\xi_{y(j)(k)}) - (u_{zs}(y(j)) - u_{zs}(y(k))) J_{\tau s}^{44} g_2^2(\xi_{y(j)(k)}) \end{array} \right\} \Delta L_{(j)} = P_z^{\tau} \quad (21)$$

On the boundary, Equation (15) yields

$$\sum_{j=1}^{N(k)} \left\{ \begin{array}{l} (u_{xs}(y(j)) - u_{xs}(y(k))) J_{\tau s}^{66} n_y g_2^1(\xi_{y(j)(k)}) \\ + u_{ys}(y(j)) J_{\tau s, x}^{66} n_y g_2^0(\xi_{y(j)(k)}) \end{array} \right\} \Delta L_{(j)} = \bar{p}_x^{\tau} \quad (22)$$

$$\sum_{j=1}^{N(k)} \left\{ \begin{array}{l} u_{xs}(y(j)) J_{\tau s, x}^{21} n_y g_2^0(\xi_{y(j)(k)}) \\ + (u_{ys}(y(j)) - u_{ys}(y(k))) J_{\tau s}^{22} n_y g_2^1(\xi_{y(j)(k)}) \\ + u_{zs}(y(j)) J_{\tau s, z}^{23} n_y g_2^0(\xi_{y(j)(k)}) \end{array} \right\} \Delta L_{(j)} = \bar{p}_y^{\tau} \quad (23)$$

$$\sum_{j=1}^{N(k)} \left\{ \begin{array}{l} u_{ys}(y(j)) J_{\tau s, z}^{44} n_y g_2^0(\xi_{y(j)(k)}) \\ + (u_{zs}(y(j)) - u_{zs}(y(k))) J_{\tau s}^{44} n_y g_2^1(\xi_{y(j)(k)}) \end{array} \right\} \Delta L_{(j)} = \bar{p}_z^{\tau} \quad (24)$$

where $\Delta L_{(j)}$ is the length of grid spacing, as the 1D equivalence of volume. According to Equation (7), g_2^0 , g_2^1 , g_2^2 are PD functions for solution of the 0th, 1st and 2nd order partial derivatives. For PDDO numerical implementation, Equations (19)–(24) are rewritten in component wise form as given in Equations (A21)–(A28). The proposed unified dimensionally reduced approach is implemented with Intel Fortran compiler 2025.2 in Windows 11 system. Results are visualized through ParaView 6.0.

4. Numerical results

This section investigates the capability of the unified approach with PDDO in restoring 3D deformation states with 1D models, by considering 3D beam structures subjected to various boundary conditions. 1D PDDO computational models, along with the corresponding boundary conditions, are illustrated to differentiate the mathematical surface enabled by Taylor expansion class and the physical surface enabled by Lagrange expansion class. The advantages of two expansion methods are demonstrated through comparisons against analytical solutions (approximate equations

for the deflection curve of Euler-Bernoulli beams) and finite element predictions.

4.1. Simple tension tests

As shown in Figures 5 and 8, a beam ($L = 50, M = D = 10$, unit: mm) is uniformly discretized into 50 particles along y -direction, with the grid size $\Delta = 1$ mm. A Cartesian system is located at the left end of the beam along y -direction. For 4.1.1 and 4.1.2, the 1D PDDO models are expanded by TE and LE respectively. 3D PDDO(TE_1) and PDDO(LE_1 \times 1 L4) beam models are constructed as shown in Figure 5(a) and 5(b). The beam is isotropic with Young's modulus of 70 GPa and the Poisson's ratio of 0.3. The horizon is specified as $\delta = 3\Delta$ and the weight function is specified as $w(\xi) = e^{-(4\xi/\delta)^2}$.

4.1.1. Simple tension tests—displacement boundary

As shown in Figure 5(a), the PDDO(LE_1 \times 1 L4) model possesses physical surfaces. The displacement boundary $\bar{u}_y = 0.5$ mm is applied directly on the surface nodes. The BCs are applied as

$$\left. \begin{array}{l} u_y(x, y, z) = 0 \\ \sigma_{yx}(x, y, z) = 0 \\ \sigma_{yz}(x, y, z) = 0 \end{array} \right\} \text{for } y = 0$$

$$\left. \begin{array}{l} u_y(x, y, z) = \bar{u}_y \\ \sigma_{yx}(x, y, z) = 0 \\ \sigma_{yz}(x, y, z) = 0 \end{array} \right\} \text{for } y = L \quad (25)$$

$$\left. \begin{array}{l} u_x(x, y, z) = 0 \\ u_z(x, y, z) = 0 \end{array} \right\} \text{for } x = -W/2, z = -D/2$$

$$u_z(x, y, z) = 0 \quad \text{for } x = W/2, z = -D/2.$$

The PDDO(TE_1) model (Figure 5(b)) generates mathematical surfaces based on centered expansion, whose BCs are applied as

$$\left. \begin{aligned}
 u_{x\tau}(x, y, z) = 0, \tau = 1 \\
 u_{y\tau}(x, y, z) = 0, \tau = 1 \\
 u_{z\tau}(x, y, z) = 0, \tau = 1 \\
 \sigma_{yx}(x, y, z) = 0 \\
 \sigma_{yz}(x, y, z) = 0 \\
 u_{x\tau}(x, y, z) = 0, \tau = 1 \\
 u_{y\tau}(x, y, z) = \bar{u}_y, \tau = 1 \\
 u_{z\tau}(x, y, z) = 0, \tau = 1 \\
 \sigma_{yx}(x, y, z) = 0 \\
 \sigma_{yz}(x, y, z) = 0
 \end{aligned} \right\} \begin{array}{l} \text{for } y = 0 \\ \\ \\ \text{for } y = L. \end{array} \quad (26)$$

The BCs on other surfaces are automatically satisfied which are thereby omitted for simplicity. To enable the same bulk behavior, PDDO(LE) model restrains surface nodes while PDDO(TE) model restrains the central particles on the boundaries, as illustrated in Figure 5.

As shown in Figure 6, displacement components predicted by PDDO are compared with analytical solutions and FEM results. The analytical expressions for Figure 6(d)–(f) are, respectively, $u_z = 1.0 \times 10^{-2} y$, $u_x = -3 \times 10^{-3} x$ and $u_z = -3 \times 10^{-3} z$ (unit: mm, PDDO(TE) models take the middle plane as reference plane). CUF(LE_1 \times 1 L4) model with 50 B2 elements along y -direction is utilized for FEM analysis [31]. PDDO(TE) and PDDO(LE) models are able to restore the 3D deformation states of beam structures (Figure 6(a)–(c)), which are identical to analytical results and FEM results (Figure 6(d)–(f)). Given a non-uniformly discretized model, PDDO recovers its 3D deformation states as well, as depicted in Figure 7(a) and (b).

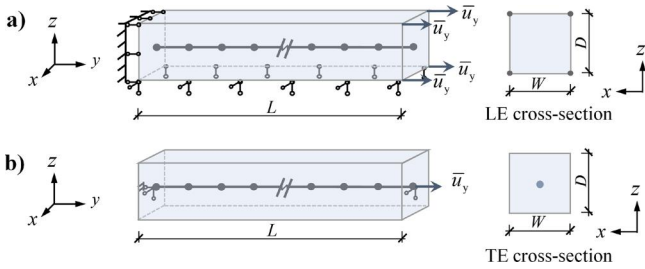


Figure 5. The geometry of ST-D models: (a) 3D PDDO(LE_1 \times 1 L4) beam model, (b) 3D PDDO(TE_1) beam model.

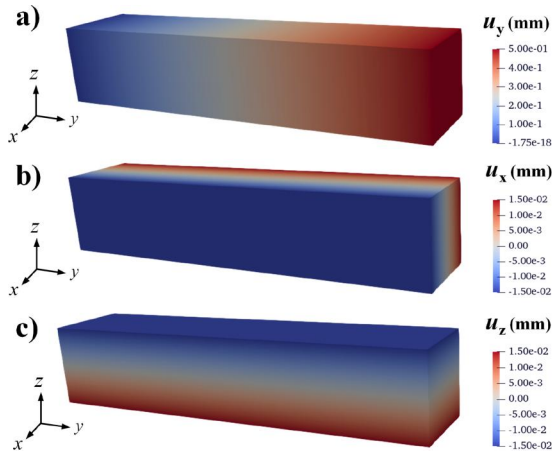


Figure 6. Displacement components predicted by PDDO(TE_1) models: (a) u_y , (b) u_x , (c) u_z ; Comparison of displacements along (d) $x = 0, z = D/2$, (e) $y = L/2, z = D/2$, (f) $x = W/2, y = L/2$ in ST-D tests.

4.1.2. Simple tension tests—traction boundary

For the simple tension tests—traction boundary tests, the right end of the beam is subjected to a traction of $\bar{p}_y = 500$ MPa. BCs applied on the PDDO(LE_1 \times 1 L4) model (Figure 8(a)) are

$$\left. \begin{aligned}
 u_y(x, y, z) = 0 \\
 \sigma_{yx}(x, y, z) = 0 \\
 \sigma_{yz}(x, y, z) = 0 \\
 \sigma_{yx}(x, y, z) = 0 \\
 \sigma_{yy}(x, y, z) = \bar{p}_y \\
 \sigma_{yz}(x, y, z) = 0 \\
 u_x(x, y, z) = 0 \\
 u_z(x, y, z) = 0 \\
 u_x(x, y, z) = 0
 \end{aligned} \right\} \begin{array}{l} \text{for } y = 0 \\ \\ \\ \text{for } y = L \\ \\ \\ \text{for } x = -W/2, z = -D/2 \\ \\ \text{for } x = W/2, z = -D/2. \end{array} \quad (27)$$

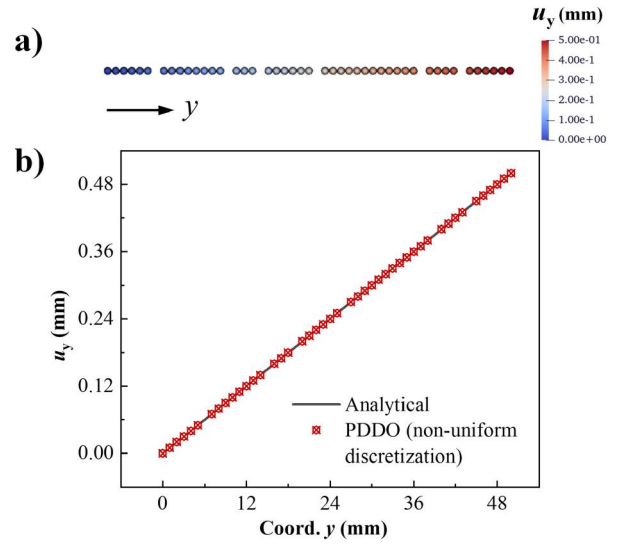
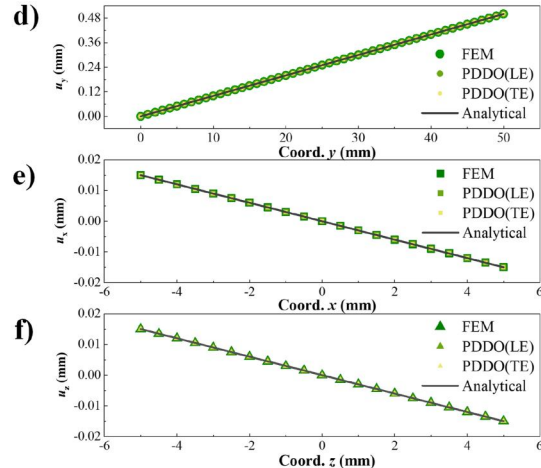


Figure 7. Displacement variations predicted by PDDO model with non-uniform discretization in ST-D tests.



For PDDO(TE₁) model (Figure 8(b)), the BCs are

$$\left. \begin{aligned} u_{x\tau}(x, y, z) &= 0, \tau = 1 \\ u_{y\tau}(x, y, z) &= 0, \tau = 1 \\ u_{z\tau}(x, y, z) &= 0, \tau = 1 \\ \sigma_{yx}(x, y, z) &= 0 \\ \sigma_{yz}(x, y, z) &= 0 \end{aligned} \right\} \text{for } y = 0 \quad (28)$$

$$\left. \begin{aligned} u_{x\tau}(x, y, z) &= 0, \tau = 1 \\ u_{z\tau}(x, y, z) &= 0, \tau = 1 \\ \sigma_{yx}(x, y, z) &= 0 \\ \sigma_{yy}(x, y, z) &= \bar{p}_y \\ \sigma_{yz}(x, y, z) &= 0 \end{aligned} \right\} \text{for } y = L.$$

The traction boundary of PDDO(TE₁) model is enabled based on Eq. (A20), while for PDDO(LE₁ × 1 L4) model it is enforced as evenly distributed nodal forces on plane $y = L$. According to Figure 9(a)–(f), PDDO, FEM results and analytical solutions agree well with each other. The analytical expressions for Figure 9(d)–(f) are, respectively, $u_z = 7.14 \times 10^{-3} y$, $u_x = -2.14 \times 10^{-3} (x + 5)$ and $u_z = -2.14 \times 10^{-3} (z + 5)$ (unit: mm, PDDO(LE) models take the surface plane as reference plane). CUF(LE₁ × 1 L4) model with 50 B2 elements along y -direction is utilized for FEM analysis. The Poisson effect in x and z directions are well revealed in 3D manner. As indicated in Figure 7(a) and (b) and Figure 10(a) and (b), PDDO enables nonuniform discretization and is free of nonlocal surface effects from the truncated domain of interaction at points near the boundary.

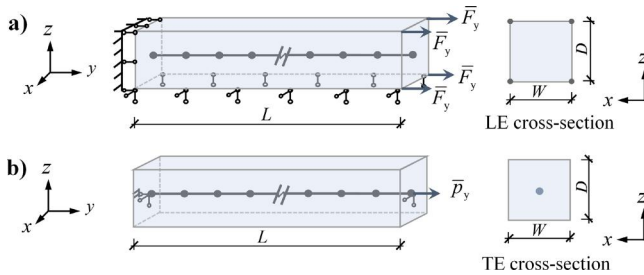


Figure 8. The geometry of ST-T models: (a) 3D PDDO(LE₁ × 1 L4) beam model, (b) 3D PDDO(TE₁) beam model.

4.1.3. Simple tension tests—3D entity and its discretizations

The PDDO(LE) model constructs a 3D entity with physical surfaces. A beam with dimensions $L = 40, M = 20, D = 2$ (unit: mm) in Figure 11(a) can be discretized into two different types of PDDO(LE₁ × 1 L4) models labeled as PDDO(LE(a)) and PDDO(LE(b)) respectively along y -direction and z -direction as illustrated in Figure 11(b) and (c). The BCs of PDDO(LE(a)) are given as

$$\left. \begin{aligned} u_y(x, y, z) &= 0 \\ \sigma_{yx}(x, y, z) &= 0 \\ \sigma_{yz}(x, y, z) &= 0 \end{aligned} \right\} \text{for } y = 0$$

$$\left. \begin{aligned} \sigma_{yx}(x, y, z) &= 0 \\ \sigma_{yy}(x, y, z) &= \bar{p}_y \\ \sigma_{yz}(x, y, z) &= 0 \end{aligned} \right\} \text{for } y = L \quad (29)$$

$$\left. \begin{aligned} u_x(x, y, z) &= 0 \\ u_z(x, y, z) &= 0 \end{aligned} \right\} \text{for } x = -W/2, z = -D/2$$

$$u_z(x, y, z) = 0 \quad \text{for } x = W/2, z = -D/2$$

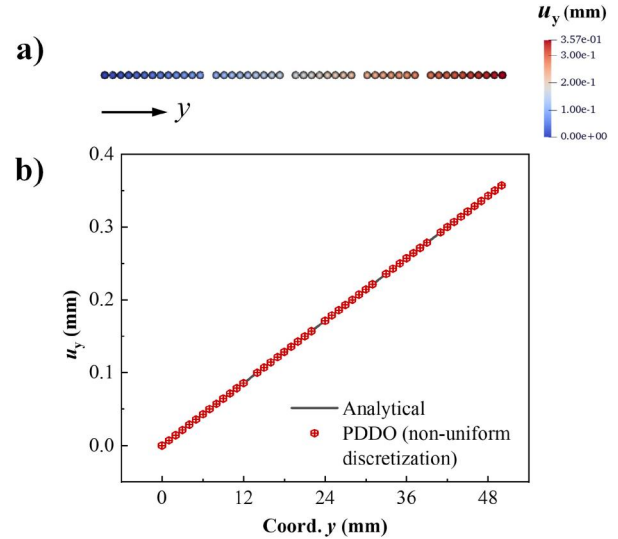


Figure 10. Displacement variations predicted by PDDO model with non-uniform discretization in ST-T tests.

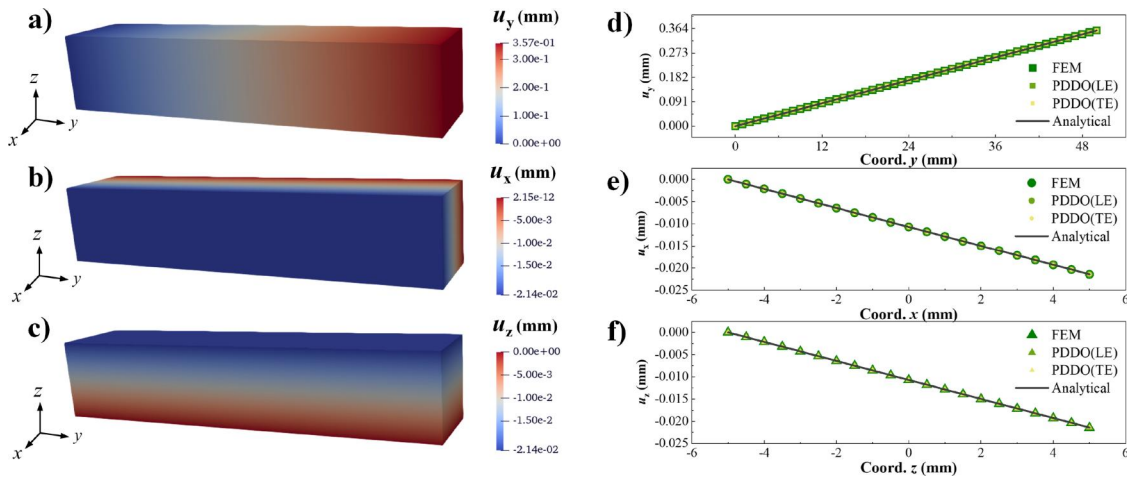


Figure 9. Displacement components predicted by PDDO(LE₁ × 1 L4) models: (a) u_y , (b) u_x , (c) u_z ; Comparison of displacements along (d) $x = 0, z = D/2$, (e) $y = L/2, z = D/2$, (f) $x = W/2, y = L/2$ in ST-T tests.

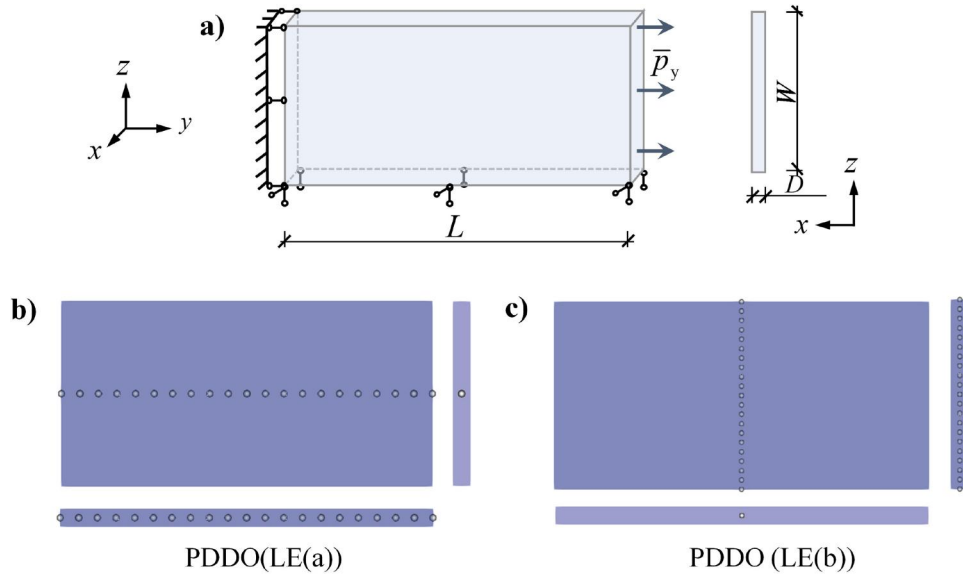


Figure 11. The ST-AB model and its discretizations: (a) model geometry; (b) PDDO(LE(a)) model, (c) PDDO(LE(b)) model.

where $\bar{p}_y = 500$ MPa. The BCs of PDDO(LE(b)) are

$$\left. \begin{aligned}
 & \left. \begin{aligned}
 u_y(x, y, z) = 0 \\
 \sigma_{yx}(x, y, z) = 0 \\
 \sigma_{yz}(x, y, z) = 0
 \end{aligned} \right\} \text{for } y = 0 \\
 & \left. \begin{aligned}
 \sigma_{yx}(x, y, z) = 0 \\
 \sigma_{yy}(x, y, z) = \bar{p}_y \\
 \sigma_{yz}(x, y, z) = 0
 \end{aligned} \right\} \text{for } y = L \\
 & \left. \begin{aligned}
 u_x(x, y, z) = 0 \\
 u_z(x, y, z) = 0
 \end{aligned} \right\} \text{for } x = -W/2, z = -D/2 \\
 & u_z(x, y, z) = 0 \quad \text{for } x = W/2, z = -D/2 \\
 & \left. \begin{aligned}
 \sigma_{zx}(x, y, z) = 0 \\
 \sigma_{zy}(x, y, z) = 0 \\
 \sigma_{zz}(x, y, z) = 0
 \end{aligned} \right\} \text{for } z = W/2 \\
 & \left. \begin{aligned}
 \sigma_{zx}(x, y, z) = 0 \\
 \sigma_{zy}(x, y, z) = 0 \\
 \sigma_{zz}(x, y, z) = 0
 \end{aligned} \right\} \text{for } z = -W/2.
 \end{aligned} \right\} \quad (30)$$

As indicated in Figure 11(b) and (c), LE model variables and BCs can be located directly on the physical surfaces. Without rotations or higher-order variables, pure displacement components are taken as the unknown variables, which provides enhanced flexibility for the discretization of beam-type structures and is able to meet a wider range of modeling needs. The traction boundaries can therefore be applied as nodal forces in different ways as shown in PDDO(LE(a)) model and PDDO(LE(b)) model. Displacement variations predicted by PDDO(LE) models are compared in Figure 12. The analytical expressions for Figure 12(a)–(c) are $u_y = 7.14 \times 10^{-3} y$, $u_x = -2.14 \times 10^{-3} (x + 10)$ and $u_z = -2.14 \times 10^{-3} (z + 1)$ (unit: mm). CUF(LE_1

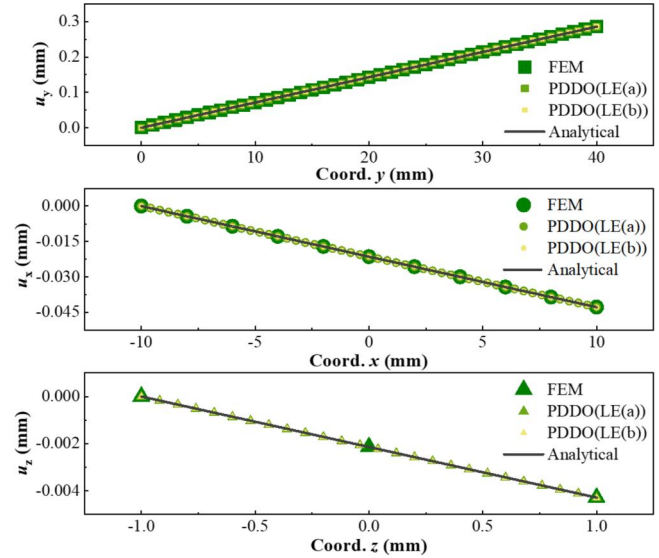


Figure 12. Comparison of displacement variations along (a) $x = D/2, z = W/2$; (b) $y = L/2, x = D/2$; (c) $y = L/2, z = W/2$ in ST-AB tests.

$\times 1$ L4) model with 50 B2 elements along discretization direction is utilized for FEM analysis. According to Figure 12, PDDO(LE) results are identical to analytical solutions and FEM results, verifying the capability of PDDO(LE) approach for reproducing 3D deformation states of beam-type structures.

4.2. Bending tests

4.2.1. Bending tests—line load

With the same beam geometry as Sec. 4.1, PDDO(LE_2 \times 2 L4) and PDDO(TE_3) models with 1000 PD particles are utilized for the bending tests. The BCs of bending tests—

line load tests are illustrated in Figure 13 ($\bar{q}_z = -200$ N/mm). For PDDO(LE) model, line loads are enforced as nodal forces and the BCs are given as

$$\left. \begin{aligned} u_x(x, y, z) &= 0 \\ u_y(x, y, z) &= 0 \\ u_z(x, y, z) &= 0 \end{aligned} \right\} \text{ for } y = 0 \quad (31)$$

$$P_z(x, y, z) = \bar{P}_z \quad \text{for } z = D/2, y = L.$$

For PDDO(TE) beam model, BCs are given as

$$\left. \begin{aligned} u_{x\tau}(x, y, z) &= 0, \tau = 1, 2, \dots, N \\ u_{y\tau}(x, y, z) &= 0, \tau = 1, 2, \dots, N \\ u_{z\tau}(x, y, z) &= 0, \tau = 1, 2, \dots, N \end{aligned} \right\} \text{ for } y = 0 \quad (32)$$

$$q_z(x, y, z) = \bar{q}_z \quad \text{for } z = D/2, y = L.$$

The line loads are applied based on Eq. (A20) for PDDO(TE) analysis. For the construction of PDDO, third-order TS is utilized; thus, the horizon is set $\delta = (3 + 1)\Delta$. Displacements predicted by PDDO models are in agreement with analytical and FEM results (Figure 14(a)–(f)). The analytical expression for Figure 14(d) is $u_z = -8.57 \times 10^{-4}y^2 + 5.71 \times 10^{-6}y^3$ (unit: mm). CUF(LE_2 \times 2 L4) model with 1000 B2 elements along y -direction is utilized for FEM analysis. Stress and strain variations along path $x = W/2, y = L/2$ and path $y = L/2, z = D/2$ are depicted respectively in Figure 15(a) and (b). PDDO results are in agreement with the analytical solutions (the analytical expressions for Figure 15(a) and (b) are $\epsilon_{yy} = 4.29 \times 10^{-3}$ and $\sigma_{yy} = -60z$, unit: MPa) and FEM results.

4.2.2. Bending tests—moment boundary

The 3D TE beam model discretizes the bulk model with a system of particles with mass density, which pertains to the

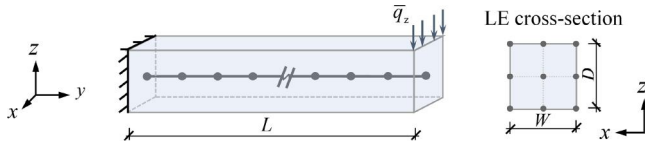


Figure 13. The geometry of BD-L model.

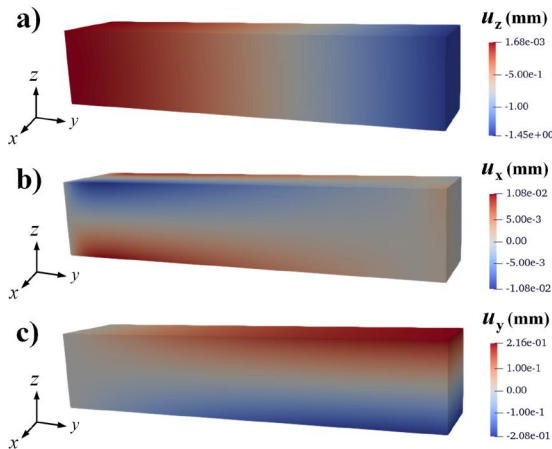


Figure 14. Displacement components predicted by PDDO(TE) models: (a) u_z , (b) u_x , (c) u_y ; Comparison of displacements along (d) $x = 0, z = D/2$, (e) $y = L/2, z = D/2$, (f) $x = W/2, y = L/2$ in BD-L tests.

static and dynamic simulations of beam structures with 3D geometric characteristics. For a simply supported beam (Figure 16), boundary conditions can be applied on certain particles directly in the form of body load. The BCs are written as

$$\left. \begin{aligned} u_{x\tau}(x, y, z) &= 0, \tau = 1 \\ u_{y\tau}(x, y, z) &= 0, \tau = 1 \\ u_{z\tau}(x, y, z) &= 0, \tau = 1 \\ M_x(x, y, z) &= -\bar{M}_x \end{aligned} \right\} \text{ for } y = 0 \quad (33)$$

$$\left. \begin{aligned} u_{x\tau}(x, y, z) &= 0, \tau = 1 \\ u_{z\tau}(x, y, z) &= 0, \tau = 1 \\ M_x(x, y, z) &= \bar{M}_x \end{aligned} \right\} \text{ for } y = L$$

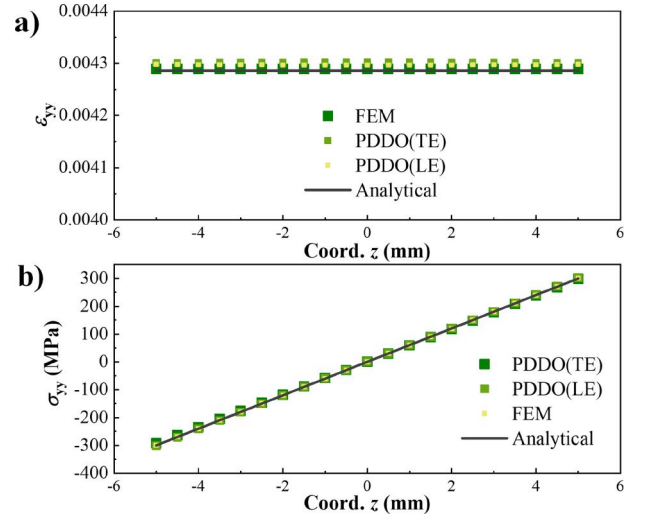


Figure 15. Strain and stress variations along (a) path $y = L/2, z = D/2$ and (b) path $x = W/2, y = L/2$ in BD-L tests.

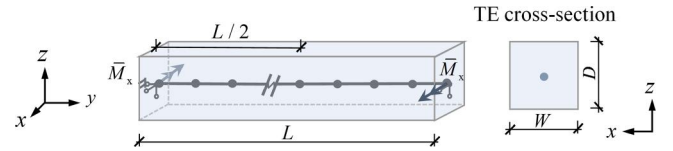
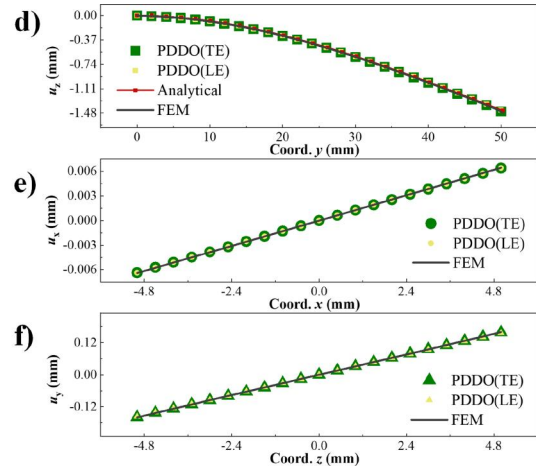


Figure 16. The geometry of BD-M model.



where $\bar{M}_x = 5.6 \times 10^5 \text{ N} \cdot \text{mm}$. The displacement variations predicted by PDDO(TE_3), FEM and analytical solutions are depicted in Figure 17(a) and (b). The analytical expression for Figure 17(b) is $u_z = 4.8 \times 10^{-3} y^2 - 2.4 \times 10^{-1} y$ (unit: mm). CUF(TE_3) model with 1000 B2 elements along y -direction is utilized for FEM analysis. PDDO and FEM results are in agreement with the analytical solution. Moreover, as shown in Figure 18(a) and (b), the PDDO(TE) model can capture the stress variations in conformity with FEM results and analytical solutions. The analytical expressions for Figure 18(b) are $\epsilon_{yy} = -3.36 \times 10^3$ for $z = D/2$ and $\epsilon_{yy} = +3.36 \times 10^3$ for $z = -D/2$ (unit: MPa).

4.3. Box beam

Figure 19(a) shows the geometry ($L = 50, M = 10, D = 10, t = 1$, unit: mm) and the boundary conditions ($\bar{u}_z = -5$ mm) of the box beam. The model is composed of 1000 particles in y -direction. The cross-sections are established by Taylor expansion (Figure 19(b): PDDO(TE_3), $N = 1, 3, 5, 7, 9$) or Lagrange expansion (Figure 19(c): PDDO(LE_8L4), PDDO(LE_12L4), PDDO(LE_20L4),

PDDO(LE_36L4), PDDO(LE_12L9)). The BCs of the PDDO(LE) beam models are

$$\left. \begin{aligned} u_x(x, y, z) &= 0 \\ u_y(x, y, z) &= 0 \\ u_z(x, y, z) &= 0 \end{aligned} \right\} \text{ for } y = 0 \quad (34)$$

$$\left. \begin{aligned} u_y(x, y, z) &= 0 \\ u_z(x, y, z) &= \bar{u}_z \end{aligned} \right\} \text{ for } y = L,$$

while for PDDO(TE) beam models there give

$$\left. \begin{aligned} u_{x\tau}(x, y, z) &= 0, \tau = 1, 2, \dots, N \\ u_{y\tau}(x, y, z) &= 0, \tau = 1, 2, \dots, N \\ u_{z\tau}(x, y, z) &= 0, \tau = 1, 2, \dots, N \end{aligned} \right\} \text{ for } y = 0 \quad (35)$$

$$\left. \begin{aligned} u_{y\tau}(x, y, z) &= 0, \tau = 1 \\ u_{z\tau}(x, y, z) &= \bar{u}_z, \tau = 1 \end{aligned} \right\} \text{ for } y = L.$$

Paths P1 ($x = 0, z = 5$), P2 ($y = 6, z = 5$), P3 ($y = 6, x = 4$) and P4 ($y = 6, z = 4$) are specified for discussion, as shown in Figure 19. Figures 20 and 21 depict the displacement variations predicted by PDDO(TE_9), PDDO(LE_36L4), PDDO(LE_12L9) and FEM along path P1 and P2.

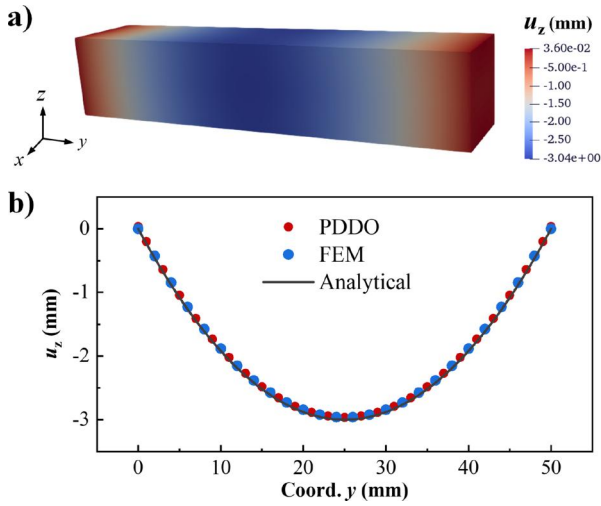


Figure 17. Displacement variations along $x = 0, z = D/2$ in BD-M tests.

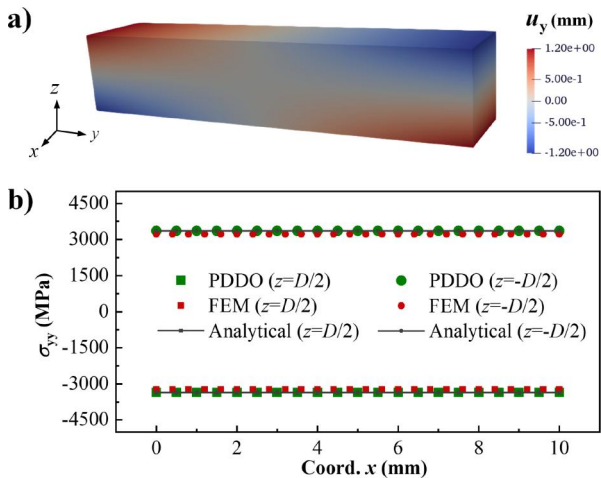


Figure 18. Stress variations along $y = L/2, z = \pm D/2$ in BD-M tests.

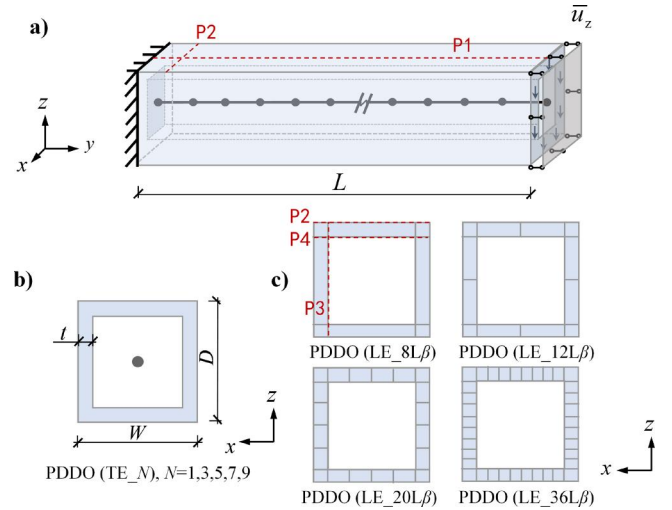


Figure 19. The box-beam and its cross-sectional expansions: (a) model geometry; (b) PDDO(TE) cross-sections; (c) PDDO(LE) cross-sections.

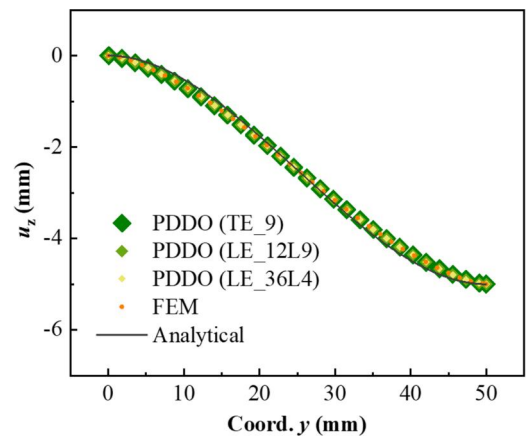


Figure 20. Displacement variations of the box beam along path P1.

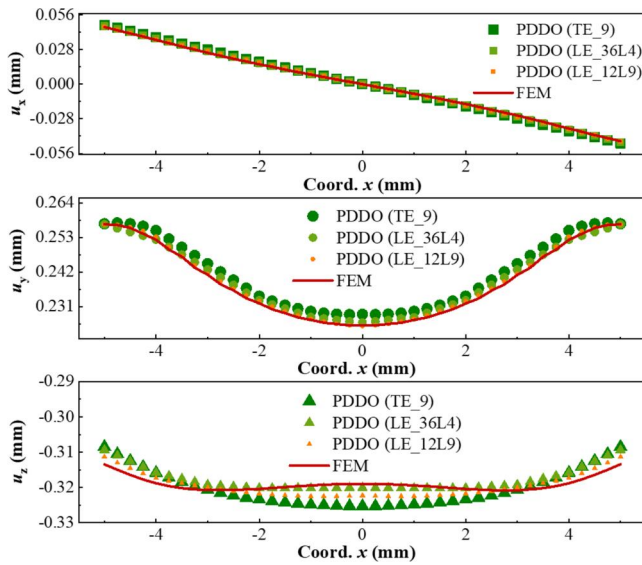


Figure 21. Displacement variations of the box beam along path P2.

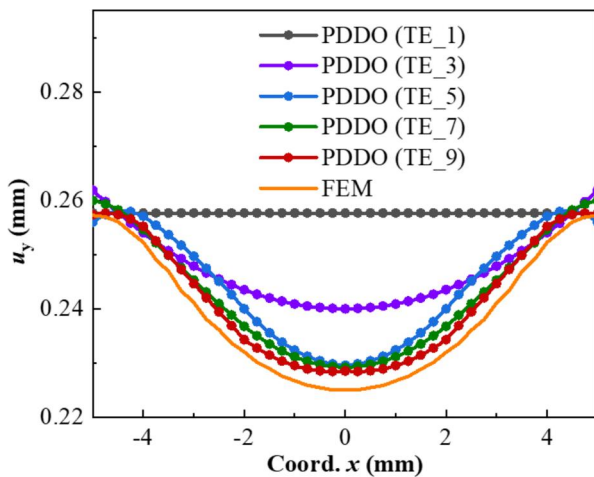


Figure 22. Displacements predicted by PDDO (TE class) models along path P2.

The overall deformation of box beam can be characterized by z -displacement variation along P1. As indicated in Figure 20, all three PDDO models are capable of reproducing FEM results and show modest differences with the analytical solution. The analytical expression for Figure 20 is $u_z = 8 \times 10^{-5} y^3 - 6 \times 10^{-3} y^2$ (unit: mm). FEM analysis is conducted on ABAQUS (84335 C3D8R elements). Since the box beam has notable 3D characteristics, further analysis is conducted in comparison with FEM predictions. From a detailed perspective, as compared in Figure 21 along P2, PDDO(LE) models are more effective in capturing the finer displacement variations, which indicates that for beam-type structures with complex geometries local approximation schemes like Lagrange expansions are more effective than the global expansions *via* Taylor polynomials. For PDDO(TE) models (Figure 22), the increase of Taylor expansion order contributes to more accurate results, which is referred to as p -refinement. While for PDDO(LE) models in Figure 23 (PDDO(LE_8L4), PDDO(LE_12L4), PDDO(LE_20L4), PDDO(LE_36L4)), better accuracy can be achieved through mesh refinement, referred to as h -

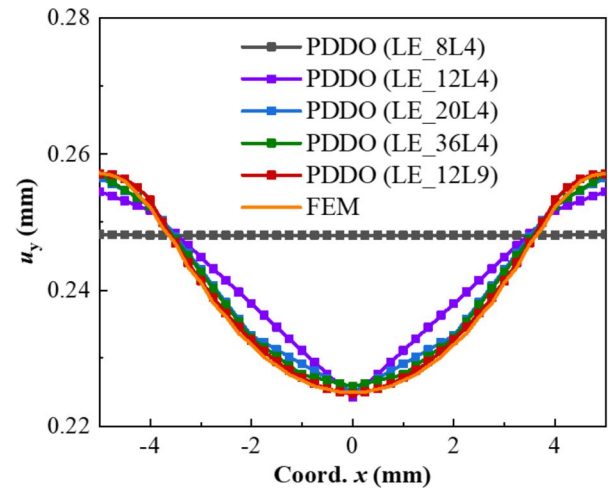


Figure 23. Displacements predicted by PDDO (LE class) models along path P2.

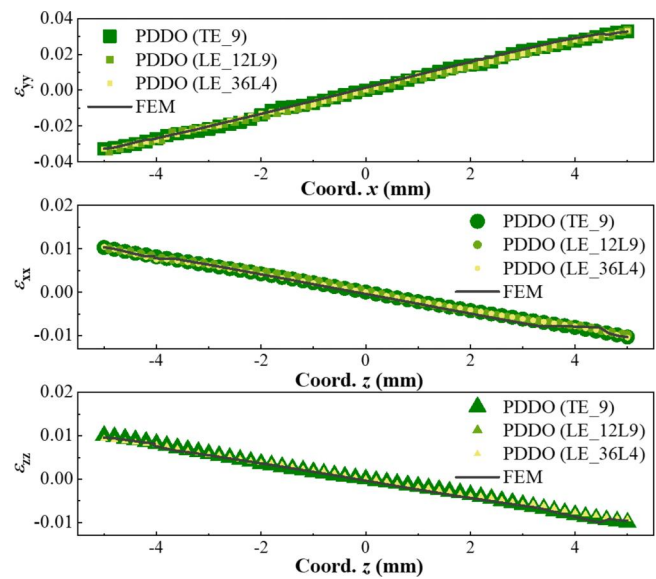


Figure 24. Strain variations along path P3.

refinement. Higher-order PDDO(LE_12L9) model shares the same number of cross-sectional unknowns with PDDO(LE_36L4) model, however, according to Figure 23, PDDO(LE_12L9) generates smoother displacement curve and shows better convergence performance than that of PDDO(LE_36L4) model. Modest discrepancies in strain variations along P3 and P4 between two models arise from numerical instability and are respectively observed at different curve sections to the reference data, as shown in Figures 24 and 25. Therefore, the accuracy of PDDO(LE) approach depends not only on the number of unknowns, but also on the order of expansion, node distribution and numerical stability. The comparison among PDDO(LE) models as depicted in Figure 23 also implies the hp -refinement feature of the proposed PDDO(LE) approach.

5. Conclusions

This study incorporates the PDDO approach in CUF to model beam-type structures with 3D characteristics. The

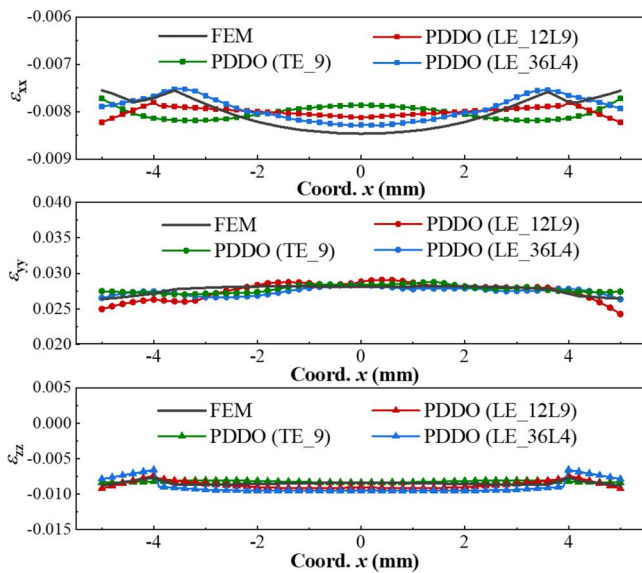


Figure 25. Strain variations along path P4.

construction of full 3D entities through Taylor or Lagrange expansion classes within the unified formulation of high-order beam theories facilitates the straightforward application of boundary conditions. The extraction of PDDO fundamental nuclei enables automated assembly and efficient numerical implementation on digital computers. Two types of 3D models are developed to accommodate diverse practical scenarios, such as beam-type structures with different geometric characteristics, various boundary conditions and non-uniform discretizations. Compared with the conventional FEM, the proposed approach effectively reconstructs 3D deformation responses from 1D PDDO models.

Acknowledgments

The first author would like to express gratitude to the MUL2 Lab at Politecnico di Torino.

Author contributions

CRedit: **Jing Zhang**: Conceptualization, Methodology, Software, Validation, Visualization, Writing – original draft, Writing – review & editing; **Erdogan Madenci**: Supervision, Writing – review & editing; **Yijun Liu**: Supervision, Writing – review & editing.

Disclosure statement

No potential conflict of interest was reported by the authors.

ORCID

Jing Zhang  <http://orcid.org/0009-0007-8941-8444>

Data availability

Data available on request from the authors.

References

- [1] K.-J. Bathe, *Finite Element Procedures*, Prentice Hall, New Jersey, 1996. <https://api.semanticscholar.org/CorpusID:118162737>.
- [2] E. Madenci, A. Barut, and M. Dorduncu, *Peridynamic Differential Operator for Numerical Analysis*, Springer, Cham, 2019. DOI: [10.1007/978-3-030-02647-9](https://doi.org/10.1007/978-3-030-02647-9).
- [3] S.A. Silling, Reformulation of elasticity theory for discontinuities and long-range forces, *J. Mech. Phys. Solids*, vol. 48, no. 1, pp. 175–209, 2000. DOI: [10.1016/S0022-5096\(99\)00029-0](https://doi.org/10.1016/S0022-5096(99)00029-0).
- [4] S.A. Silling, M. Epton, O. Weckner, J. Xu, and E. Askari, Peridynamic states and constitutive modeling, *J. Elasticity*, vol. 88, no. 2, pp. 151–184, 2007. DOI: [10.1007/s10659-007-9125-1](https://doi.org/10.1007/s10659-007-9125-1).
- [5] S.A. Silling, Peridynamic theory of solid mechanics, *Adv. Appl. Mech.*, vol. 44, pp. 73–168, 2010. DOI: [10.1016/S0065-2156\(10\)44002-8](https://doi.org/10.1016/S0065-2156(10)44002-8).
- [6] P.R. Budarapu, and T. Rabczuk, Multiscale methods for fracture: a review, *J. Indian Inst. Sci.*, vol. 97, no. 3, pp. 339–376, 2017. DOI: [10.1007/s41745-017-0041-5](https://doi.org/10.1007/s41745-017-0041-5).
- [7] S.A. Silling, and R.B. Lehoucq, Convergence of peridynamics to classical elasticity theory, *J. Elasticity*, vol. 93, no. 1, pp. 13–37, 2008. DOI: [10.1007/s10659-008-9163-3](https://doi.org/10.1007/s10659-008-9163-3).
- [8] P. Seleson, M.L. Parks, M. Gunzburger, and R.B. Lehoucq, Peridynamics as an upscaling of molecular dynamics, *Multiscale Model. Simul.*, vol. 8, no. 1, pp. 204–227, 2009. DOI: [10.1137/09074807X](https://doi.org/10.1137/09074807X).
- [9] E. Madenci, A. Barut, and M. Futch, Peridynamic differential operator and its applications, *Comput. Methods Appl. Mech. Eng.*, vol. 304, pp. 408–451, 2016. DOI: [10.1016/j.cma.2016.02.028](https://doi.org/10.1016/j.cma.2016.02.028).
- [10] E. Madenci, P. Roy, and D. Behera, *Advances in Peridynamics*, Springer, Switzerland, 2022. DOI: [10.1007/978-3-030-97858-7](https://doi.org/10.1007/978-3-030-97858-7).
- [11] E. Madenci, A. Barut, M. Dorduncu, and N.D. Phan, Coupling of peridynamics with finite elements without an overlap zone, In *2018 AIAA/ASCE/AHS/ASC Structures, Structural Dynamics, and Materials Conference*. American Institute of Aeronautics and Astronautics, Kissimmee, FL, 2018. DOI: [10.2514/6.2018-1462](https://doi.org/10.2514/6.2018-1462).
- [12] E. Madenci, M. Dorduncu, A. Barut, and N. Phan, Weak form of peridynamics for nonlocal essential and natural boundary conditions, *Comput. Methods Appl. Mech. Eng.*, vol. 337, pp. 598–631, 2018. DOI: [10.1016/j.cma.2018.03.038](https://doi.org/10.1016/j.cma.2018.03.038).
- [13] E. Madenci, M. Dorduncu, N. Phan, and X. Gu, Weak form of bond-associated non-ordinary state-based peridynamics free of zero energy modes with uniform or non-uniform discretization, *Eng. Fract. Mech.*, vol. 218, pp. 106613, 2019. DOI: [10.1016/j.engfracmech.2019.106613](https://doi.org/10.1016/j.engfracmech.2019.106613).
- [14] S.V.K. Anicode, and E. Madenci, Seamless coupling of bond-and state-based peridynamic and finite element analyses, *Mech. Mater.*, vol. 173, pp. 104433, 2022. DOI: [10.1016/j.mechmat.2022.104433](https://doi.org/10.1016/j.mechmat.2022.104433).
- [15] D. Behera, P. Roy, S.V.K. Anicode, E. Madenci, and B. Spencer, Imposition of local boundary conditions in peridynamics without a fictitious layer and unphysical stress concentrations, *Comput. Methods Appl. Mech. Eng.*, vol. 393, pp. 114734, 2022. DOI: [10.1016/j.cma.2022.114734](https://doi.org/10.1016/j.cma.2022.114734).
- [16] M. D'Elia, X. Li, P. Seleson, X. Tian, and Y. Yu, A review of local-to-nonlocal coupling methods in nonlocal diffusion and nonlocal mechanics, *J. Peridyn. Nonlocal Model.*, vol. 4, no. 1, pp. 1–50, 2022. DOI: [10.1007/s42102-020-00038-7](https://doi.org/10.1007/s42102-020-00038-7).
- [17] M. Dorduncu, H. Ren, X. Zhuang, S. Silling, E. Madenci, and T. Rabczuk, A review of peridynamic theory and nonlocal operators along with their computer implementations, *Comput. Struct.*, vol. 299, pp. 107395, 2024. DOI: [10.1016/j.compstruc.2024.107395](https://doi.org/10.1016/j.compstruc.2024.107395).
- [18] E. Oterkus, and S. Oterkus, Recent advances in peridynamic theory: a review, *AIMSMATES*, vol. 11, no. 3, pp. 515–546, 2024. DOI: [10.3934/matserci.2024026](https://doi.org/10.3934/matserci.2024026).

- [19] E. Madenci, S.V.K. Anicode, and Y. Zhang, *Peridynamics and Its Applications Using Ansys*, Springer, Cham, 2024. DOI: [10.1007/978-3-031-59896-8](https://doi.org/10.1007/978-3-031-59896-8).
- [20] S.A. Silling, M. Zimmermann, and R. Abeyaratne, Deformation of a peridynamic bar, *J. Elast.*, vol. 73, no. 1-3, pp. 173–190, 2003. DOI: [10.1023/B:ELAS.0000029931.03844.4f](https://doi.org/10.1023/B:ELAS.0000029931.03844.4f).
- [21] S.A. Silling, and F. Bobaru, Peridynamic modeling of membranes and fibers, *Int. J. Non. Linear Mech.*, vol. 40, no. 2-3, pp. 395–409, 2005. DOI: [10.1016/j.ijnonlinmec.2004.08.004](https://doi.org/10.1016/j.ijnonlinmec.2004.08.004).
- [22] Z.Y. Aung, D. Vo, P. Suttakul, E. Atroshchenko, T.Q. Bui, and J. Rungamornrat, Peridynamic formulations for planar arbitrarily curved beams with Euler-Bernoulli beam model, *Thin. Walled Struct.*, vol. 204, pp. 112278, 2024. DOI: [10.1016/j.tws.2024.112278](https://doi.org/10.1016/j.tws.2024.112278).
- [23] D.V. Nguyen, P. Suttakul, M.N. Nguyen, E. Madenci, T.Q. Bui, J. Rungamornrat, and D. Vo, On invariant and locking-free formulations for planar arbitrarily curved beams with Timoshenko-Ehrenfest beam model and peridynamic differential operator, *Comput. Struct.*, vol. 309, pp. 107658, 2025. DOI: [10.1016/j.compstruc.2025.107658](https://doi.org/10.1016/j.compstruc.2025.107658).
- [24] Z. Li, D. Huang, K. Yan, and Y. Xu, Large deformation analysis of functionally graded beam with variable cross-section by using peridynamic differential operator, *Compos. Struct.*, vol. 279, pp. 114788, 2022. DOI: [10.1016/j.compstruct.2021.114788](https://doi.org/10.1016/j.compstruct.2021.114788).
- [25] E. Madenci, M. Dorduncu, A. Barut, and N.D. Phan, Progressive failure analysis of composites based on peridynamics and refined zigzag theory, In *AIAA Scitech 2019 Forum*. American Institute of Aeronautics and Astronautics, San Diego, CA, 2019. DOI: [10.2514/6.2019-1039](https://doi.org/10.2514/6.2019-1039).
- [26] M. Dorduncu, Stress analysis of laminated composite beams using refined zigzag theory and peridynamic differential operator, *Compos. Struct.*, vol. 218, pp. 193–203, 2019. DOI: [10.1016/j.compstruct.2019.03.035](https://doi.org/10.1016/j.compstruct.2019.03.035).
- [27] M. Dorduncu, Peridynamic modeling of adhesively bonded beams with modulus graded adhesives using refined zigzag theory, *Int. J. Mech. Sci.*, vol. 185, pp. 105866, 2020. DOI: [10.1016/j.ijmecsci.2020.105866](https://doi.org/10.1016/j.ijmecsci.2020.105866).
- [28] J. Zhang, A. Pagani, E. Madenci, Q. Yang, and E. Carrera, Peridynamic differential operator for solution of high-order beam and plate equations, *Int. J. Mech. Sci.*, vol. 302, pp. 110240, 2025. DOI: [10.1016/j.ijmecsci.2025.110240](https://doi.org/10.1016/j.ijmecsci.2025.110240).
- [29] E. Carrera, G. Giunta, and M. Petrolo, A modern and compact way to formulate classical and advanced beam, *Dev. Comput. Struct. Technol. Ch.*, vol. 4, pp. 75–112, 2010. DOI: [10.4203/cs.25.4](https://doi.org/10.4203/cs.25.4).
- [30] E. Carrera, and G. Giunta, Refined beam theories based on a unified formulation, *Int. J. Appl. Mech.*, vol. 2, no. 1, pp. 117–143, 2010. DOI: [10.1142/S1758825110000500](https://doi.org/10.1142/S1758825110000500).
- [31] E. Carrera, M. Cinefra, M. Petrolo, and E. Zappino, *Finite Element Analysis of Structures Through Unified Formulation*, Wiley, Chichester, West Sussex, 2014. DOI: [10.1002/9781118536643](https://doi.org/10.1002/9781118536643).
- [32] A. Pagani, and E. Carrera, Unified formulation of geometrically nonlinear refined beam theories, *Mech. Adv. Mater. Struct.*, vol. 25, no. 1, pp. 15–31, 2018. DOI: [10.1080/15376494.2016.1232458](https://doi.org/10.1080/15376494.2016.1232458).
- [33] A. Pagani, E. Carrera, R. Augello, and D. Scano, Use of Lagrange polynomials to build refined theories for laminated beams, plates and shells, *Compos. Struct.*, vol. 276, pp. 114505, 2021. DOI: [10.1016/j.compstruct.2021.114505](https://doi.org/10.1016/j.compstruct.2021.114505).
- [34] Y. Yang, A. Pagani, and E. Carrera, Exact solutions for free vibration analysis of laminated, box and sandwich beams by refined layer-wise theory, *Compos. Struct.*, vol. 175, pp. 28–45, 2017. DOI: [10.1016/j.compstruct.2017.05.003](https://doi.org/10.1016/j.compstruct.2017.05.003).
- [35] A.J.M. Ferreira, C.M.C. Roque, E. Carrera, and M. Cinefra, Analysis of thick isotropic and cross-ply laminated plates by radial basis functions and a unified formulation, *J. Sound Vib.*, vol. 330, no. 4, pp. 771–787, 2011. DOI: [10.1016/j.jsv.2010.08.037](https://doi.org/10.1016/j.jsv.2010.08.037).
- [36] A.J.M. Ferreira, C.M.C. Roque, E. Carrera, M. Cinefra, and O. Polit, Bending and vibration of laminated plates by a layerwise formulation and collocation with radial basis functions, *Mech. Adv. Mater. Struct.*, vol. 20, no. 8, pp. 624–637, 2013. DOI: [10.1080/15376494.2011.643282](https://doi.org/10.1080/15376494.2011.643282).
- [37] A. Pagani, E. Carrera, and A.J.M. Ferreira, Higher-order theories and radial basis functions applied to free vibration analysis of thin-walled beams, *Mech. Adv. Mater. Struct.*, vol. 23, no. 9, pp. 1080–1091, 2016. DOI: [10.1080/15376494.2015.1121555](https://doi.org/10.1080/15376494.2015.1121555).
- [38] A. Pagani, and E. Carrera, Coupling three-dimensional peridynamics and high-order one-dimensional finite elements based on local elasticity for the linear static analysis of solid beams and thin-walled reinforced structures, *Num. Meth. Eng.*, vol. 121, no. 22, pp. 5066–5081, 2020. DOI: [10.1002/nme.6510](https://doi.org/10.1002/nme.6510).
- [39] J. Zhang, M. Enea, A. Pagani, E. Carrera, E. Madenci, X. Liu, and Q. Yang, A computational approach to integrate three-dimensional peridynamics and two-dimensional higher-order classical elasticity theory for fracture analysis, *Eng. Comput.*, vol. 41, no. 1, pp. 335–351, 2025. DOI: [10.1007/s00366-024-02001-2](https://doi.org/10.1007/s00366-024-02001-2).

Appendix A: CUF-PDDO fundamental nuclei for beam type structures

The governing equations and the fundamental nuclei in CCM form are obtained through PVD

$$\delta L_{\text{int}} = \delta L_{\text{ext}}, \quad (\text{A1})$$

where L_{int} denotes the internal strain energy and L_{ext} denotes the work due to external loadings. Given the unified formulation based on high order beam theories

$$\mathbf{u} = F_s \mathbf{u}_s, s = 1, 2, \dots, M, \quad (\text{A2})$$

the displacement components u_x , u_y , u_z and their relative variations are

$$\begin{aligned} (u_x, u_y, u_z) &= F_s (u_{xs}, u_{ys}, u_{zs}) \\ (\delta u_x, \delta u_y, \delta u_z) &= F_\tau (\delta u_{x\tau}, \delta u_{y\tau}, \delta u_{z\tau}). \end{aligned} \quad (\text{A3})$$

Linear strain-displacement relations are written as

$$\begin{aligned} \boldsymbol{\epsilon}_p &= [\epsilon_{xx}, \epsilon_{zz}, \gamma_{zx}]^T = \mathbf{D}_p \mathbf{u} \\ \boldsymbol{\epsilon}_n &= [\epsilon_{yy}, \gamma_{yz}, \gamma_{xy}]^T = (\mathbf{D}_{np} + \mathbf{D}_{nn}) \mathbf{u}, \end{aligned} \quad (\text{A4})$$

where the differential operator matrices in explicit form are

$$\mathbf{D}_p = \begin{bmatrix} \frac{\partial}{\partial x} & 0 & 0 \\ 0 & 0 & \frac{\partial}{\partial z} \\ \frac{\partial}{\partial z} & 0 & \frac{\partial}{\partial x} \end{bmatrix}, \quad \mathbf{D}_{np} = \begin{bmatrix} 0 & 0 & 0 \\ 0 & \frac{\partial}{\partial z} & 0 \\ 0 & \frac{\partial}{\partial x} & 0 \end{bmatrix}, \quad \mathbf{D}_{nn} = \begin{bmatrix} 0 & \frac{\partial}{\partial y} & 0 \\ 0 & 0 & \frac{\partial}{\partial y} \\ \frac{\partial}{\partial y} & 0 & 0 \end{bmatrix}. \quad (\text{A5})$$

The constitutive equations are

$$\begin{aligned} \boldsymbol{\sigma}_p &= [\sigma_{xx}, \sigma_{zz}, \tau_{zx}]^T = \mathbf{C}_{pp} \boldsymbol{\epsilon}_p + \mathbf{C}_{pn} \boldsymbol{\epsilon}_n \\ \boldsymbol{\sigma}_n &= [\sigma_{yy}, \tau_{yz}, \tau_{xy}]^T = \mathbf{C}_{np} \boldsymbol{\epsilon}_p + \mathbf{C}_{nn} \boldsymbol{\epsilon}_n \end{aligned} \quad (\text{A6})$$

with

$$\begin{aligned} \mathbf{C}_{pp} &= \begin{bmatrix} C_{11} & C_{13} & 0 \\ C_{13} & C_{33} & 0 \\ 0 & 0 & C_{55} \end{bmatrix}, \quad \mathbf{C}_{nn} = \begin{bmatrix} C_{22} & 0 & 0 \\ 0 & C_{44} & 0 \\ 0 & 0 & C_{66} \end{bmatrix}, \\ \mathbf{C}_{pn} = \mathbf{C}_{np}^T &= \begin{bmatrix} C_{12} & 0 & 0 \\ C_{23} & 0 & 0 \\ 0 & 0 & 0 \end{bmatrix}, \end{aligned} \quad (\text{A7})$$

where

$$\begin{aligned} C_{11} = C_{22} = C_{33} &= \frac{1-\nu}{(1+\nu)(1-2\nu)}E \\ C_{12} = C_{13} = C_{23} &= \frac{\nu}{(1+\nu)(1-2\nu)}E \\ C_{44} = C_{55} = C_{66} &= \frac{1}{2(1+\nu)}E. \end{aligned} \quad (\text{A8})$$

The virtual variation of the strain energy is considered as the sum of two

$$\delta L_{\text{int}} = \int_{\Omega} \int_l \delta \boldsymbol{\epsilon}_n^T \boldsymbol{\sigma}_n dld\Omega + \int_l \int_{\Omega} \delta \boldsymbol{\epsilon}_p^T \boldsymbol{\sigma}_p d\Omega dl, \quad (\text{A9})$$

where Ω and l are integration domains of xz plane and y direction, respectively. Stress $\boldsymbol{\sigma}$ and strain $\boldsymbol{\epsilon}$ vectors are decomposed as cross-section components and through-length components, denoted by the subscripts p and n . Substituting geometric relations, constitutive equations and the unified formulation into the variational form of PVD leads to

$$\begin{aligned} \delta L_{\text{int}} &= \int_l \int_{\Omega} [(\mathbf{D}_p F_\tau \delta \mathbf{u}_\tau)^T (\mathbf{C}_{pp} \mathbf{D}_p F_s \mathbf{u}_s + \mathbf{C}_{pn} (\mathbf{D}_{np} + \mathbf{D}_{nn}) F_s \mathbf{u}_s) \\ &\quad + ((\mathbf{D}_{np} + \mathbf{D}_{nn}) F_\tau \delta \mathbf{u}_\tau)^T (\mathbf{C}_{np} \mathbf{D}_p F_s \mathbf{u}_s + \mathbf{C}_{nn} (\mathbf{D}_{np} + \mathbf{D}_{nn}) F_s \mathbf{u}_s)] d\Omega dl. \end{aligned} \quad (\text{A10})$$

After integration by parts, Eq. (A10) yields

$$\begin{aligned} \delta L_{\text{int}} &= \int_l \int_{\Omega} (\delta \mathbf{u}_\tau)^T [\mathbf{D}_p^T (\mathbf{C}_{pp} \mathbf{D}_p + \mathbf{C}_{pn} (\mathbf{D}_{np} + \mathbf{D}_{nn})) \\ &\quad + (\mathbf{D}_{np} - \mathbf{D}_{nn})^T (\mathbf{C}_{np} \mathbf{D}_p + \mathbf{C}_{nn} (\mathbf{D}_{np} + \mathbf{D}_{nn}))] F_\tau F_s \mathbf{u}_s d\Omega dl \\ &\quad + \int_l \int_{\Omega} (\delta \mathbf{u}_\tau)^T [\mathbf{I}_{nn}^T (\mathbf{C}_{np} \mathbf{D}_p + \mathbf{C}_{nn} (\mathbf{D}_{np} + \mathbf{D}_{nn}))] F_\tau F_s \mathbf{u}_s d\Omega dl, \end{aligned} \quad (\text{A11})$$

where

$$\mathbf{I}_{nn} = \begin{bmatrix} 0 & n_y & 0 \\ 0 & 0 & n_y \\ n_y & 0 & 0 \end{bmatrix} \quad (\text{A12})$$

with $n_y = \cos(\varphi_y)$. The angle between the normal direction and y -direction is φ_y . The virtual variation of strain energy in compact form is given as

$$\delta L_{\text{int}} = \int_l (\delta \mathbf{u}_\tau^T \mathbf{K}^{\text{ts}} \mathbf{u}_s + \delta \mathbf{u}_\tau^T \Pi^{\text{ts}} \mathbf{u}_s) dl. \quad (\text{A13})$$

The fundamental nuclei \mathbf{K}^{ts} and Π^{ts} are expressed as

$$\mathbf{K}^{\text{ts}} = \int_{\Omega} [\mathbf{D}_p^T (\mathbf{C}_{pp} \mathbf{D}_p + \mathbf{C}_{pn} (\mathbf{D}_{np} + \mathbf{D}_{nn})) + (\mathbf{D}_{np} - \mathbf{D}_{nn})^T (\mathbf{C}_{np} \mathbf{D}_p + \mathbf{C}_{nn} (\mathbf{D}_{np} + \mathbf{D}_{nn}))] d\Omega \quad (\text{A14})$$

$$\Pi^{\text{ts}} = \int_{\Omega} [\mathbf{I}_{nn}^T (\mathbf{C}_{np} \mathbf{D}_p + \mathbf{C}_{nn} (\mathbf{D}_{np} + \mathbf{D}_{nn}))] d\Omega, \quad (\text{A15})$$

which can be written in explicit form as

$$\begin{aligned} K_{11}^{\text{ts}} &= J_{\tau, x^s, x}^{11} + J_{\tau, z^s, z}^{55} - J_{\tau s}^{66} \frac{\partial^2}{\partial y^2} \\ K_{12}^{\text{ts}} &= \left(J_{\tau, x^s}^{12} - J_{\tau s, x}^{66} \right) \frac{\partial}{\partial y} \\ K_{13}^{\text{ts}} &= J_{\tau, x^s, z}^{13} + J_{\tau, z^s, x}^{55} \\ K_{21}^{\text{ts}} &= \left(J_{\tau, x^s}^{66} - J_{\tau s, x}^{12} \right) \frac{\partial}{\partial y} \\ K_{22}^{\text{ts}} &= J_{\tau, x^s, x}^{66} + J_{\tau, z^s, z}^{44} - J_{\tau s}^{22} \frac{\partial^2}{\partial y^2} \\ K_{23}^{\text{ts}} &= \left(J_{\tau, z^s}^{44} - J_{\tau s, z}^{23} \right) \frac{\partial}{\partial y} \\ K_{31}^{\text{ts}} &= J_{\tau, x^s, z}^{55} + J_{\tau, z^s, x}^{13} \\ K_{32}^{\text{ts}} &= \left(J_{\tau, z^s}^{23} - J_{\tau s, z}^{44} \right) \frac{\partial}{\partial y} \\ K_{33}^{\text{ts}} &= J_{\tau, x^s, x}^{55} + J_{\tau, z^s, z}^{33} - J_{\tau s}^{44} \frac{\partial^2}{\partial y^2} \end{aligned} \quad (\text{A16})$$

$$\begin{aligned} \Pi_{11}^{\text{ts}} &= J_{\tau s}^{66} n_y \frac{\partial}{\partial y}, \quad \Pi_{12}^{\text{ts}} = J_{\tau s, x}^{66} n_y, \quad \Pi_{13}^{\text{ts}} = 0 \\ \Pi_{21}^{\text{ts}} &= J_{\tau s, x}^{12} n_y, \quad \Pi_{22}^{\text{ts}} = J_{\tau s}^{22} n_y \frac{\partial}{\partial y}, \quad \Pi_{23}^{\text{ts}} = J_{\tau s, z}^{23} n_y \\ \Pi_{31}^{\text{ts}} &= 0, \quad \Pi_{32}^{\text{ts}} = J_{\tau s, z}^{44} n_y, \quad \Pi_{33}^{\text{ts}} = J_{\tau s}^{44} n_y \frac{\partial}{\partial y}. \end{aligned} \quad (\text{A17})$$

In addition, the virtual variation of the external work contributed by inner particles and boundary particles are also presented for reference, which are expressed as

$$\delta L_{\text{ext}} = \int_l (\delta \mathbf{u}_\tau^T \mathbf{P}^\tau + \delta \mathbf{u}_\tau^T \bar{\mathbf{p}}^\tau) dl, \quad (\text{A18})$$

where \mathbf{P}^τ is the force vector of inner particles and $\bar{\mathbf{p}}^\tau$ is the force vector of boundary particles. For the applied displacement $\bar{\mathbf{u}}$, $\bar{\mathbf{p}}^\tau$ can be written as

$$\bar{\mathbf{p}}^\tau = \Pi^{\text{ts}} \bar{\mathbf{u}}_s. \quad (\text{A19})$$

For the external transversal pressure $\bar{\boldsymbol{\sigma}}$, $\bar{\mathbf{p}}^\tau$ can be written as

$$\bar{\mathbf{p}}^\tau = \int_{\Omega} F_\tau d\Omega \bar{\boldsymbol{\sigma}}. \quad (\text{A20})$$

For the point-wise force $\bar{\mathbf{F}}$ loaded at (x_0, y_0, z_0) , $\bar{\mathbf{p}}^\tau$ is enforced as the combination of a concentrated force and a torque depending on the location of $\bar{\mathbf{F}}$, as elaborated in Ref. [31].

For PDDO implementation, rewrite Equation (19)–(21) in the form of PD functions as

$$\begin{bmatrix} P_{x(k)}^\tau \\ P_{y(k)}^\tau \\ P_{z(k)}^\tau \\ P_{x(j)}^\tau \\ P_{y(j)}^\tau \\ P_{z(j)}^\tau \end{bmatrix} = \sum_{j \in H(k)} \begin{bmatrix} \Phi_{(k)(j)}^{(1,1)} & \Phi_{(k)(j)}^{(1,2)} & \Phi_{(k)(j)}^{(1,3)} & \Phi_{(k)(j)}^{(1,4)} & \Phi_{(k)(j)}^{(1,5)} & \Phi_{(k)(j)}^{(1,6)} \\ \Phi_{(k)(j)}^{(2,1)} & \Phi_{(k)(j)}^{(2,2)} & \Phi_{(k)(j)}^{(2,3)} & \Phi_{(k)(j)}^{(2,4)} & \Phi_{(k)(j)}^{(2,5)} & \Phi_{(k)(j)}^{(2,6)} \\ \Phi_{(k)(j)}^{(3,1)} & \Phi_{(k)(j)}^{(3,2)} & \Phi_{(k)(j)}^{(3,3)} & \Phi_{(k)(j)}^{(3,4)} & \Phi_{(k)(j)}^{(3,5)} & \Phi_{(k)(j)}^{(3,6)} \\ 0 & 0 & 0 & 0 & 0 & 0 \\ 0 & 0 & 0 & 0 & 0 & 0 \\ 0 & 0 & 0 & 0 & 0 & 0 \end{bmatrix} \begin{bmatrix} u_{xs}(Y(k)) \\ u_{ys}(Y(k)) \\ u_{zs}(Y(k)) \\ u_{xs}(Y(j)) \\ u_{ys}(Y(j)) \\ u_{zs}(Y(j)) \end{bmatrix}, \quad (\text{A21})$$

where

$$\begin{aligned} \Phi_{(k)(j)}^{(1,1)} &= J_{\tau s}^{66} g_2^2(\xi_{y(j)(k)}) \Delta L_{(j)} \\ \Phi_{(k)(j)}^{(1,2)} &= -\left(J_{\tau, x^s}^{12} - J_{\tau s, x}^{66} \right) g_2^1(\xi_{y(j)(k)}) \Delta L_{(j)} \\ \Phi_{(k)(j)}^{(1,3)} &= 0 \\ \Phi_{(k)(j)}^{(1,4)} &= \left(J_{\tau, x^s, x}^{11} + J_{\tau, z^s, z}^{55} \right) g_2^0(\xi_{y(j)(k)}) \Delta L_{(j)} - J_{\tau s}^{66} g_2^2(\xi_{y(j)(k)}) \Delta L_{(j)} \\ \Phi_{(k)(j)}^{(1,5)} &= \left(J_{\tau, x^s}^{12} - J_{\tau s, x}^{66} \right) g_2^1(\xi_{y(j)(k)}) \Delta L_{(j)} \\ \Phi_{(k)(j)}^{(1,6)} &= \left(J_{\tau, x^s, z}^{13} + J_{\tau, z^s, x}^{55} \right) g_2^0(\xi_{y(j)(k)}) \Delta L_{(j)} \\ \Phi_{(k)(j)}^{(2,1)} &= -\left(J_{\tau, x^s}^{66} - J_{\tau s, x}^{12} \right) g_2^1(\xi_{y(j)(k)}) \Delta L_{(j)} \\ \Phi_{(k)(j)}^{(2,2)} &= J_{\tau s}^{22} g_2^2(\xi_{y(j)(k)}) \Delta L_{(j)} \\ \Phi_{(k)(j)}^{(2,3)} &= -\left(J_{\tau, z^s}^{44} - J_{\tau s, z}^{23} \right) g_2^1(\xi_{y(j)(k)}) \Delta L_{(j)} \\ \Phi_{(k)(j)}^{(2,4)} &= \left(J_{\tau, x^s}^{66} - J_{\tau s, x}^{12} \right) g_2^1(\xi_{y(j)(k)}) \Delta L_{(j)} \\ \Phi_{(k)(j)}^{(2,5)} &= \left(J_{\tau, x^s, x}^{66} + J_{\tau, z^s, z}^{44} \right) g_2^0(\xi_{y(j)(k)}) \Delta L_{(j)} - J_{\tau s}^{22} g_2^2(\xi_{y(j)(k)}) \Delta L_{(j)} \\ \Phi_{(k)(j)}^{(2,6)} &= \left(J_{\tau, z^s}^{44} - J_{\tau s, z}^{23} \right) g_2^1(\xi_{y(j)(k)}) \Delta L_{(j)} \end{aligned} \quad (\text{A22})$$

$$\Phi_{(k)(j)}^{(2,4)} = \left(J_{\tau, x^s}^{66} - J_{\tau s, x}^{12} \right) g_2^1(\xi_{y(j)(k)}) \Delta L_{(j)} \quad (\text{A23})$$

$$\begin{aligned}
\Phi_{(k)(j)}^{(3,1)} &= 0 \\
\Phi_{(k)(j)}^{(3,2)} &= -\left(J_{\tau,z^s}^{23} - J_{\tau,z}^{44}\right)g_2^1(\zeta_{y(j)(k)})\Delta L_{(j)} \\
\Phi_{(k)(j)}^{(3,3)} &= J_{\tau s}^{44}g_2^2(\zeta_{y(j)(k)})\Delta L_{(j)} \\
\Phi_{(k)(j)}^{(3,4)} &= \left(J_{\tau,z^s,x}^{13} + J_{\tau,x^s,z}^{55}\right)g_2^0(\zeta_{y(j)(k)})\Delta L_{(j)} \\
\Phi_{(k)(j)}^{(3,5)} &= \left(J_{\tau,z^s}^{23} - J_{\tau,z}^{44}\right)g_2^1(\zeta_{y(j)(k)})\Delta L_{(j)} \\
\Phi_{(k)(j)}^{(3,6)} &= \left(J_{\tau,z^s,z}^{33} + J_{\tau,x^s,x}^{55}\right)g_2^0(\zeta_{y(j)(k)})\Delta L_{(j)} - J_{\tau s}^{44}g_2^2(\zeta_{y(j)(k)})\Delta L_{(j)}
\end{aligned} \tag{A24}$$

As defined in Equation (7), g_2^0 , g_2^1 , g_2^2 are PD functions for the 0th, 1st and 2nd order partial derivatives. Accordingly, Equation (22)–(24) on the boundary are recast into

$$\left\{ \begin{array}{l} \bar{p}_{x(k)}^\tau \\ \bar{p}_{y(k)}^\tau \\ \bar{p}_{z(k)}^\tau \\ \bar{p}_{x(j)}^\tau \\ \bar{p}_{y(j)}^\tau \\ \bar{p}_{z(j)}^\tau \end{array} \right\} = \sum_{j \in H(k)} \left[\begin{array}{cccccc} \bar{\Phi}_{(k)(j)}^{(1,1)} & \bar{\Phi}_{(k)(j)}^{(1,2)} & \bar{\Phi}_{(k)(j)}^{(1,3)} & \bar{\Phi}_{(k)(j)}^{(1,4)} & \bar{\Phi}_{(k)(j)}^{(1,5)} & \bar{\Phi}_{(k)(j)}^{(1,6)} \\ \bar{\Phi}_{(k)(j)}^{(2,1)} & \bar{\Phi}_{(k)(j)}^{(2,2)} & \bar{\Phi}_{(k)(j)}^{(2,3)} & \bar{\Phi}_{(k)(j)}^{(2,4)} & \bar{\Phi}_{(k)(j)}^{(2,5)} & \bar{\Phi}_{(k)(j)}^{(2,6)} \\ \bar{\Phi}_{(k)(j)}^{(3,1)} & \bar{\Phi}_{(k)(j)}^{(3,2)} & \bar{\Phi}_{(k)(j)}^{(3,3)} & \bar{\Phi}_{(k)(j)}^{(3,4)} & \bar{\Phi}_{(k)(j)}^{(3,5)} & \bar{\Phi}_{(k)(j)}^{(3,6)} \\ 0 & 0 & 0 & 0 & 0 & 0 \\ 0 & 0 & 0 & 0 & 0 & 0 \\ 0 & 0 & 0 & 0 & 0 & 0 \end{array} \right] \left\{ \begin{array}{l} u_{xs}(\mathcal{Y}(k)) \\ u_{ys}(\mathcal{Y}(k)) \\ u_{zs}(\mathcal{Y}(k)) \\ u_{xs}(\mathcal{Y}(j)) \\ u_{ys}(\mathcal{Y}(j)) \\ u_{zs}(\mathcal{Y}(j)) \end{array} \right\}, \tag{A25}$$

where

$$\begin{aligned}
\bar{\Phi}_{(k)(j)}^{(1,1)} &= -J_{\tau s}^{66}n_y g_2^1(\zeta_{y(j)(k)})\Delta L_{(j)} \\
\bar{\Phi}_{(k)(j)}^{(1,2)} &= 0 \\
\bar{\Phi}_{(k)(j)}^{(1,3)} &= 0 \\
\bar{\Phi}_{(k)(j)}^{(1,4)} &= J_{\tau s}^{66}n_y g_2^1(\zeta_{y(j)(k)})\Delta L_{(j)} \\
\bar{\Phi}_{(k)(j)}^{(1,5)} &= J_{\tau s}^{66}n_y g_2^0(\zeta_{y(j)(k)})\Delta L_{(j)} \\
\bar{\Phi}_{(k)(j)}^{(1,6)} &= 0
\end{aligned} \tag{A26}$$

$$\begin{aligned}
\bar{\Phi}_{(k)(j)}^{(2,1)} &= 0 \\
\bar{\Phi}_{(k)(j)}^{(2,2)} &= -J_{\tau s}^{22}n_y g_2^1(\zeta_{y(j)(k)})\Delta L_{(j)} \\
\bar{\Phi}_{(k)(j)}^{(2,3)} &= 0 \\
\bar{\Phi}_{(k)(j)}^{(2,4)} &= J_{\tau s}^{12}n_y g_2^0(\zeta_{y(j)(k)})\Delta L_{(j)} \\
\bar{\Phi}_{(k)(j)}^{(2,5)} &= J_{\tau s}^{22}n_y g_2^1(\zeta_{y(j)(k)})\Delta L_{(j)} \\
\bar{\Phi}_{(k)(j)}^{(2,6)} &= J_{\tau s,z}^{23}n_y g_2^0(\zeta_{y(j)(k)})\Delta L_{(j)} \\
\bar{\Phi}_{(k)(j)}^{(3,1)} &= 0 \\
\bar{\Phi}_{(k)(j)}^{(3,2)} &= 0 \\
\bar{\Phi}_{(k)(j)}^{(3,3)} &= -J_{\tau s}^{44}n_y g_2^1(\zeta_{y(j)(k)})\Delta L_{(j)} \\
\bar{\Phi}_{(k)(j)}^{(3,4)} &= 0 \\
\bar{\Phi}_{(k)(j)}^{(3,5)} &= J_{\tau s,z}^{44}n_y g_2^0(\zeta_{y(j)(k)})\Delta L_{(j)} \\
\bar{\Phi}_{(k)(j)}^{(3,6)} &= J_{\tau s}^{44}n_y g_2^1(\zeta_{y(j)(k)})\Delta L_{(j)}.
\end{aligned} \tag{A27}$$

$$\bar{\Phi}_{(k)(j)}^{(3,3)} = -J_{\tau s}^{44}n_y g_2^1(\zeta_{y(j)(k)})\Delta L_{(j)} \tag{A28}$$